nature neuroscience

Brief Communication

https://doi.org/10.1038/s41593-025-02159-y

Sleep-dependent infraslow rhythms are evolutionarily conserved across reptiles and mammals

Received: 22 April 2025

Accepted: 27 October 2025

Published online: 29 December 2025

Check for updates

Antoine Bergel[1,2,3,18], Julien M. Schmidt[2,4,16,18], Baptiste Barrillot[4,18], Sébastien Arthaud[4], Laetitia Averty[5], Mark S. Blumberg[6], Camille Carachet[4], Angeline Clair[5], Irina Filchenko[7], Chloé Froidevaux[1], Anthony Herrel[8,9,10,11], Bertrand Massot[12], Niels C. Rattenborg[13], Markus H. Schmidt[7,14], Mickael Tanter[1], Gianina Ungurean[4,13,17] & Paul-Antoine Libourel[4,15]

By recording brain activity in seven lizard species, humans, rats and pigeons, we demonstrate an infraslow brain rhythm during sleep in all species. This rhythm is tightly coupled with eye movements, muscle tone, heart and breathing rate in lizards, with skin brightness in chameleons and with pulsatile changes in cerebrovascular volume throughout sleep in bearded dragons and during non-rapid eye movement sleep in mice. These findings indicate that the infraslow rhythm is conserved across amniotes, questioning the evolution of sleep states.

In mammals and birds, sleep encompasses a collection of behavioral, physiological and neural components that are implicated in various functions. In these endotherms, two identifiable substates of sleep occur cyclically[1] and are homeostatically regulated[2], which are as follows: rapid eye movement (REM, or active) sleep and non-REM (NREM, or quiet) sleep. NREM sleep is generally characterized by behavioral and physiological quiescence with low regular heart and breathing rates, cortical electroencephalogram (EEG) slow waves[3] and cerebral oscillations such as sleep spindles[4]. In contrast, REM sleep is generally characterized by a wake-like cortical EEG, muscle atonia, REMs, muscle twitches, irregular heart and breathing rates, increased brain temperature and loss of thermoregulatory control[5]. In addition to this ultradian cyclicity, infraslow (<0.1 Hz; >10-s periods) fluctuations occur during sleep[6–8]. During NREM sleep in humans and rodents, EEG power in the sigma band (10–15 Hz) fluctuates at infraslow frequencies, as do heart rate[6], pupil size[9], eye movements[7], thalamic norepinephrine release[10] and microarousals[11]. These infraslow rhythms may contribute to memory[12], may enable sleeping mammals to periodically monitor their environment[11] and may serve as a 'gatekeeper' for the timing of REM sleep[11]. Infraslow oscillations in cerebral blood flow and

[1]Institute Physics for Medicine Paris, INSERM, CNRS, ESPCI Paris, PSL University, Paris, France. [2]McGill University, Montreal, Quebec, Canada. [3]Laboratoire de Plasticité du Cerveau, CNRS UMR 8249, ESPCI Paris, PSL University, Paris, France. [4]Lyon Neuroscience Research Centre, Sleep Team, CNRS UMR5292, INSERM U1028, University Claude Bernard Lyon 1, University Jean-Monnet Saint-Etienne, Bron, France. [5]Plateforme Animalerie Conventionnelle et Sauvage d'Expérimentation de la Doua (ACSED), Fédération de Recherche 3728, University of Lyon, Université Claude Bernard Lyon 1, CNRS, ENS-LYON, INRAE, INSA, VetAgro Sup, Villeurbanne, France. [6]Department of Psychological and Brain Sciences, Iowa Neuroscience Institute, University of Iowa, Iowa City, IA, USA. [7]Center for Experimental Neurology, Department of Neurology, Bern University Hospital (Inselspital), University of Bern, Bern, Switzerland. [8]Mécanismes Adaptatifs et Evolution, UMR 7179, Muséum National d'Histoire Naturelle CNRS, Paris, France. [9]Department of Biology, Evolutionary Morphology of Vertebrates, Ghent University, Ghent, Belgium. [10]Functional Morphology Laboratory, Department of Biology, University of Antwerp, Antwerp, Belgium. [11]Naturhistorisches Museum Bern, Bern, Switzerland. [12]INSA Lyon, Ecole Centrale Lyon, Universite Claude Bernard Lyon 1, CPE Lyon, CNRS, INL UMR 5270, Villeurbanne, France. [13]Avian Sleep Group, Max Planck Institute for Biological Intelligence, Seewiesen, Germany. [14]Ohio Sleep Medicine Institute, Dublin, OH, USA. [15]CEFE, Univ Montpellier, CNRS, EPHE, IRD, Montpellier, France. [16]Present address: Institute of Neuroinformatics, University of Zürich and ETH Zürich, Zurich, Switzerland. [17]Present address: University of Göttingen, Göttingen, Germany. [18]These authors contributed equally: Antoine Bergel, Julien M. Schmidt, Baptiste Barrillot. e-mail: pa.libourel@cnrs.fr

cerebrospinal fluid have also been implicated in the clearance of waste products from the brain[13]. Additionally, cycling between phasic and tonic REM sleep has been reported to occur at infraslow frequencies[14].

To date, no study has described the presence of infraslow oscillations in reptiles, which occupy a key phylogenetic position within the clade Amniota[15]. Only recently, recordings from the dorsal ventricular ridge (DVR) in bearded dragons (*Pogona vitticeps*)[16–18] and Egyptian rock agamas (*Laudakia stellio*)[19], two closely related lizards, revealed alternating patterns of brain activity[16–19] that not only share features with NREM and REM sleep in mammals and birds[17,20] but also resemble the infraslow rhythm observed during NREM sleep in mammals, as suggested in ref. 6. To further explore how sleep may have evolved, we recorded brain and body signals in seven evolutionary distant lizard species, producing the most comprehensive dataset to date on reptile sleep.

We conducted 24-h wireless recordings of local field potentials (LFPs), heart rate, breathing rate, muscle tone and eye movements at room temperatures of 20–27 °C in the following seven lizard species representing the main squamate orders and suborders: the leopard gecko (*Eublepharis macularius*), tokay gecko (*Gekko gecko*), Sudan plated lizard (*Broadleysaurus major*), Argentine tegu (*Salvator merianae*), panther chameleon (*Furcifer pardalis*), Egyptian rock agama and bearded dragon (Fig. 1a–e and Supplementary Table 1). In addition, cortical EEG recordings were analyzed during NREM sleep (Fig. 1e) in pigeons (*Columba livia*) and brown rats (*Rattus norvegicus*), as well as during N2 in humans (*Homo sapiens sapiens*). Individuals across the seven lizard species reliably exhibited broadband infraslow rhythmicity. Autocorrelations revealed periodicities associated with sustained periods of inactivity, occurring during the light phase in the nocturnal/crepuscular gecko and during the dark phase in the other diurnal species (Extended Data Fig. 1). Given the lack of consensus on reptile frequency bands, we used the 10–30 Hz range, referred to here as 'beta', to allow comparison with previous studies[16,19]. The detected infraslow rhythms were highly regular within 1-h sleep segments for each lizard, but varied across individuals with median periodicities ranging from 84 to 134.5 s (mean across lizard species = 113.2 ± 6.8 s; Fig. 1f). Similar rhythms in beta power during NREM sleep were observed in human, rat and pigeon (Fig. 1f), although median periodicities were roughly half those observed in the lizards (human, 51 s; rat, 47 s; pigeon, 49 s; Fig. 1f,g). The period of the infraslow rhythm strongly correlated (R^2 = 0.88) with body temperature across species, suggesting that the shorter periods in the endotherms are related to their higher body temperatures (Fig. 1g). The beta-power infraslow rhythm observed here in reptiles (lizards and birds) resembles the infraslow rhythm previously described in mammals during NREM sleep in the narrower sigma band (10–15 Hz)[6]. We obtained similar results when LFPs were filtered in the sigma band (Extended Data Figs. 2 and 3 and Supplementary Fig. 1), suggesting a broadband infraslow rhythm in amniotes.

During NREM sleep in humans and mice, infraslow brain rhythms occur in phase with changes in heart rate[6], pupil size[9] and noradrenergic activity[10,12]. We thus examined in lizards the phase–amplitude coupling of the cerebral infraslow rhythm with several physiological processes—heart rate, breathing rate and muscle tone (Fig. 2 and Supplementary Figs. 2–12). Heart rate was strongly modulated (positively or negatively) by the phase of the infraslow rhythm in all seven lizard species (Fig. 2b,c). We also found significant phase coupling with breathing rate and muscle tone in five of the seven lizard species (Fig. 2b,c and Supplementary Figs. 3–12). We did not observe obvious or sustained limb or tail twitching during lizard sleep. Consistent with previous findings[16,19], the density of eye movements was higher during high-beta periods in six of the seven lizard species (Fig. 2b,c). Together, these results indicate that the cerebral infraslow rhythm is not only conserved but also coupled with physiological processes across lizard species, while exhibiting interspecies differences in phasing. For example, heart rate and beta power are positively correlated in most lizard species and humans, but are anticorrelated in bearded dragons, rats (Fig. 2b,c and Extended Data Fig. 4) and mice[6].

We next used functional ultrasound imaging to determine the spatial dynamics of brain activation across the infraslow cycle in a bearded dragon (Fig. 3a–c). Functional ultrasound imaging measures cerebral blood volume (CBV) with high spatiotemporal resolution (100 µm, 200 ms) in both superficial and deep regions and can be coupled with electrophysiological recordings and video recordings of behavior[21,22]. Four bearded dragons were prepared for coronal or parasagittal imaging with bilateral LFP electrodes inserted in the DVR (Fig. 3a and Extended Data Fig. 5). The global CBV signal, computed by averaging voxel activity over the whole brain (Fig. 3b and Extended Data Fig. 5), showed strong rhythmicity only during sleep, with a prominent peak in autocorrelation at 100 s in all four animals (Fig. 3g). This CBV rhythm was strongly phase-locked to the infraslow cerebral beta rhythm; the CBV rhythm led the beta rhythm by ~10 s. Functional ultrasound images over a complete 100-s cycles revealed that all brain voxels repeatedly alternated between hypoperfusion and hyperperfusion (Supplementary Video 1 and Fig. 3c). As with the infraslow beta rhythm, the CBV rhythm was absent during wake (Fig. 3g and Extended Data Figs. 6–8).

For a direct cross-species comparison, we prepared four mice for functional ultrasound imaging across anterior (n = 1) and posterior (n = 3) coronal sections, with simultaneous electrophysiological recordings in the dorsal hippocampus (Fig. 3d). During sleep, we observed an infraslow rhythmicity in the global CBV signal, with a prominent peak in the autocorrelation period at 50 s in all four mice (Fig. 3d–f), which was more prominent during NREM than REM sleep and absent during wake (Fig. 3b and Extended Data Fig. 8). Functional ultrasound images over a complete 50-s cycle also revealed that all brain voxels alternate between strong hypoperfusion and hyperperfusion (Supplementary Video 1 and Fig. 3f). Mice showed stronger coupling between beta power and the CBV signal during NREM sleep, weaker

Fig. 1 | Cerebral infraslow and temperature-dependent rhythm in reptiles and mammals. a, Three-dimensional reconstruction from MRI and CT scans of the brain (purple) and cranium (yellow) of a leopard gecko (*E. macularius*). **b**, MRI section of a leopard gecko's brain (dark gray) showing the dorsal cortex, ventricle (light gray) and DVR region (red shaded). **c**, Postsurgical CT scan of a leopard gecko's brain, showing the electrodes implanted into the DVR (red arrow). **d**, Picture of a leopard gecko with a head-mounted logger sleeping in its shelter. **e**, Left: phylogeny of the recorded species. Middle: for each species, the raw (black) and *z*-scored (color-coded) power within the beta band (10–30 Hz) over 40 min of sleep for the lizards and 9 min of NREM sleep for the mammals and the pigeon. Black arrowhead indicates local maxima. The *x* axis indicates time of day. Right: autocorrelation maps of the *z*-scored beta power using a sliding time window (Methods). The infraslow rhythm is visible as vertical stripes at 100 s in lizards and 50 s in mammals, as well as in birds. The *y* axis indicates the time of night, and *x* axis indicates the autocorrelation lag. **f**, Violin distributions of beta-power periods extracted from autocorrelation maps for each sleep bout in each species. Lizards are tested at 20–27 °C. White dots indicate the median value across all sleep bout, colored dots indicate all sleep bouts from all individuals and the gray vertical line indicates notch values. **g**, Relationship between infraslow periods and body temperature across species. Color dots indicate the mean beta-power period at a given temperature range (ambient temperature for lizards and standard body temperature for mammals and pigeons). Vertical lines indicate s.e.m. Dashed line indicates the regression line showing the exponential relationship between the period of the infraslow rhythm and temperature. The number of individuals and replicates (sleep bouts) per species in **f** and **g** is given in Supplementary Table 1 (row 'LFP/EEG'). Leop., leopard gecko; Toka., Tokay gecko; Suda., Sudan plated lizard; Arge., Argentine tegu; Pant., panther chameleon; Egyt., Egyptian rock agama; Bea., bearded dragon; Pige., pigeon; Hum., human; Rat., brown rat; MYA, million years ago.

https://doi.org/10.1038/s41593-025-02159-y

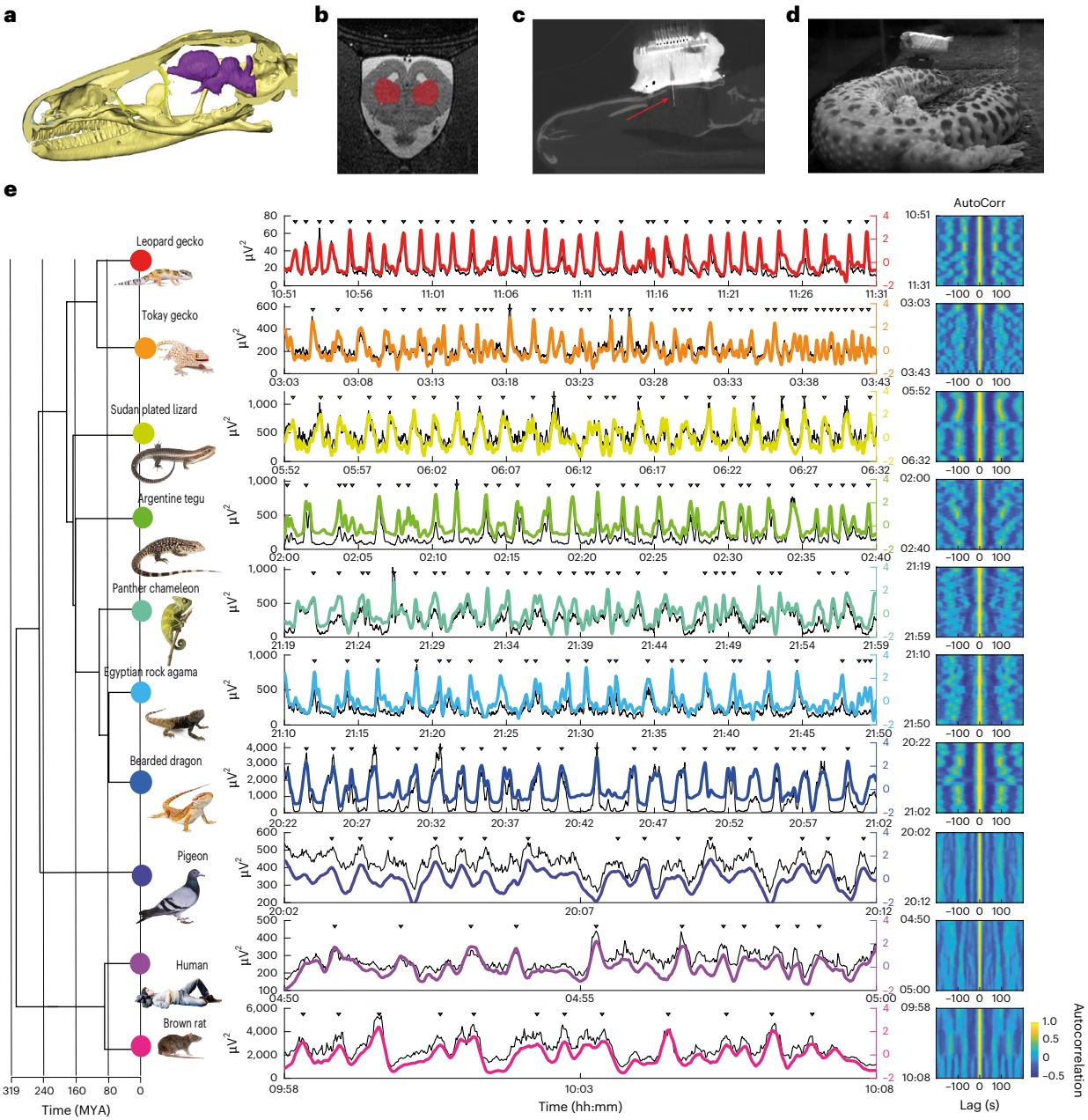

https://doi.org/10.1038/s41593-025-02159-y

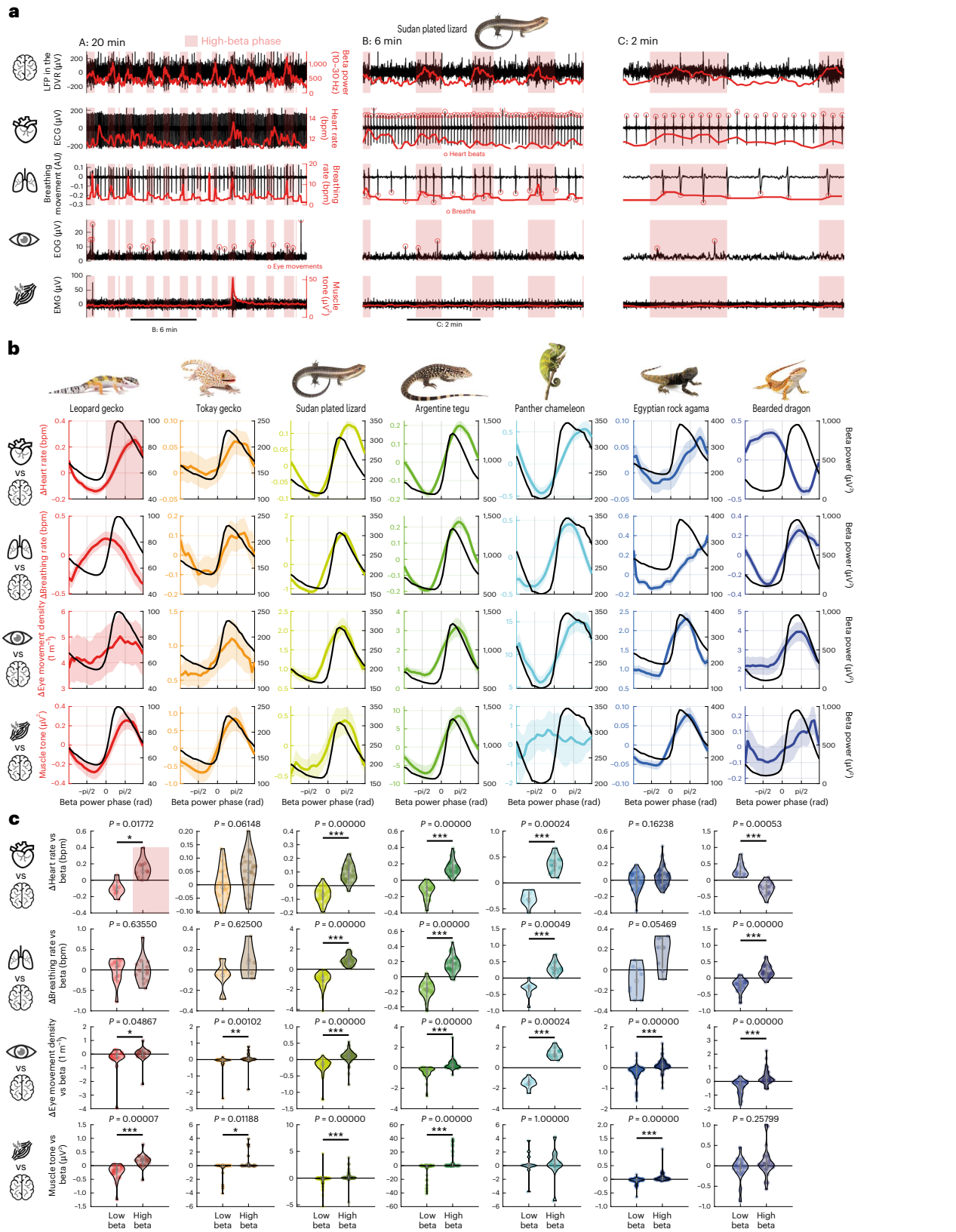

Fig. 2 | Heart rate, breathing rate, eye movements and muscle tone coupled with infraslow beta rhythm in all lizard species. a, Illustrative example in the Sudan plated lizard (*Gerrhosaurus major*) showing (top to bottom) LFPs, ECG, breathing movements, EOG and EMG. Black indicates raw traces, red indicates *z*-scored traces. Left (A): 20-min window; middle (B): 6-min box enlargement; right (C): 2-min box enlargement. Red shaded boxes represent the high phase of the beta rhythm. **b**, Mean values for heart rate, breathing rate, eye movement density and muscle tone relative to the phase of the beta rhythm, computed over all sleep bouts in all individuals in all species (solid color lines, shaded boxes—s.e.m.). The mean beta rhythm relative to its own phase is also displayed (solid black lines). Note that all physiological measures are in phase with the beta rhythm. **c**, Comparative distributions of heart rate, breathing rate, eye movement density and muscle tone between low- and high-beta-phase periods. Significant statistical differences are shown in black (**P* < 0.05 ***P* < 0 .01 ****P* < 0.001, two-sided Wilcoxon test).

https://doi.org/10.1038/s41593-025-02159-y

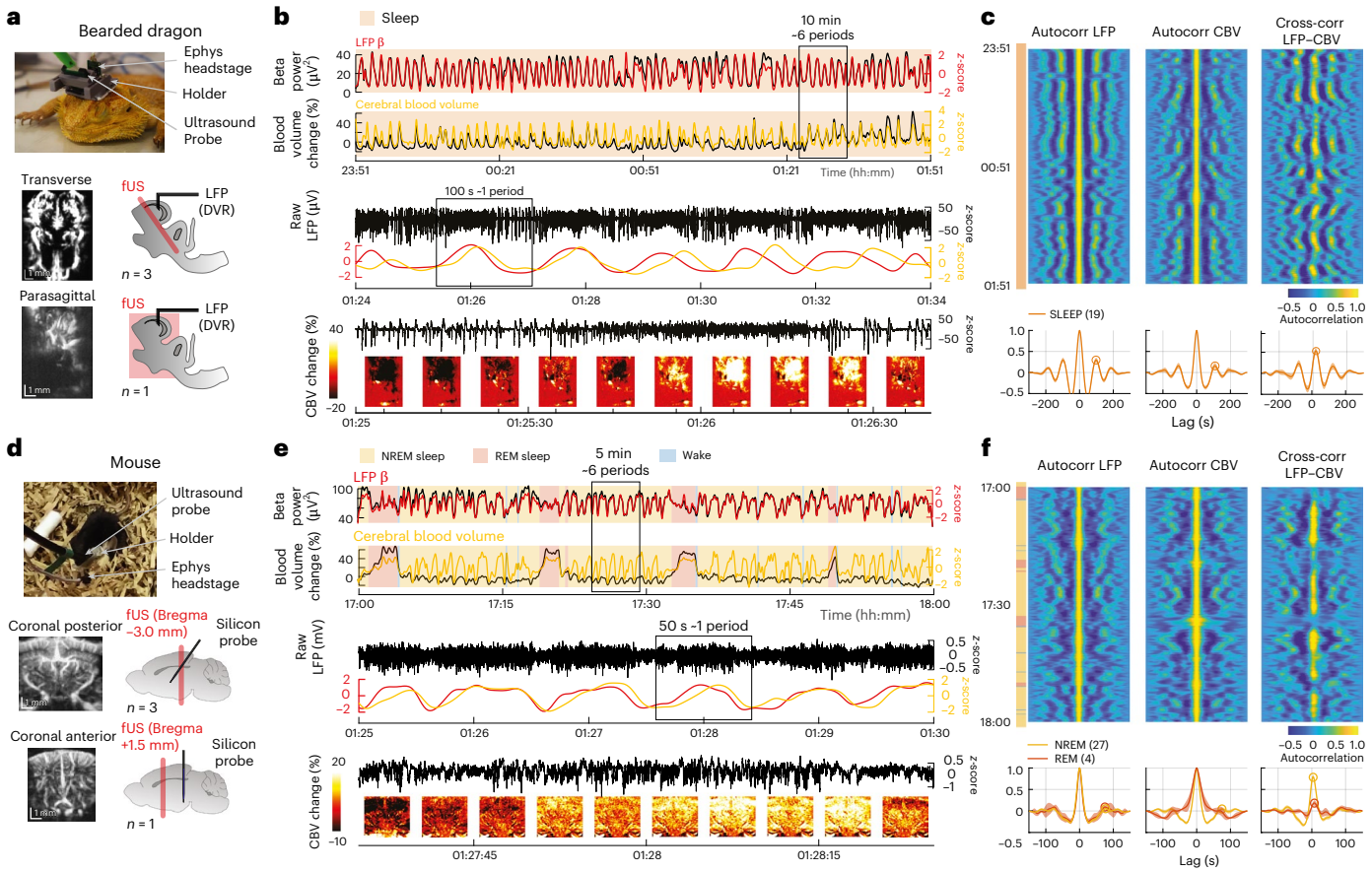

Fig. 3 | Global cerebrovascular infraslow rhythm during sleep in the bearded dragon and the mouse, coupled with brain electrophysiology. a, Top: picture of a sleeping bearded dragon equipped with the ultrasound probe and electrophysiology head stage. Bottom: ultrasound images are acquired across a transverse plane in three animals and a parasagittal plane in one animal, with electrodes in the DVR. Scale bars, 1 mm. **b**, Illustrative 2-h recording of sleep in a bearded dragon. Top: *z*-scored beta power (LFP β, red) and global CBV (yellow). Black traces indicate raw signals. Color-shaded box indicates sleep epochs. Middle: enlargement of the 10-min box showing six periods of prominent infraslow rhythm. Raw LFP is shown in black. Please note how LFP β and CBV cofluctuate with a phase shift. Bottom: enlargement of 100-s box showing one full period of infraslow rhythm, the raw LFP and the series of 10 ultrasound images taken 10 s apart. Please note how CBV rises in all brain regions during high beta. The *x* axis indicates the time of day. **c**, Autocorrelation maps of the *z*-scored beta-power (left), *z*-scored CBV (middle) and cross-correlation map between these two signals (right) using a sliding time window (Methods) for the recording shown in **b**. The *x* axis indicates lag, *y* axis indicates time and the color-shaded box indicates sleep epochs. Bottom: mean correlograms over 19 sleep bouts (shaded band, ±s.e.m.). Circles show the autocorrelation and cross-correlation positive peaks. Please note the strong coupling between LFP and CBV signals during sleep. **d**, Same as **a** for the mouse experiment. Three mice are imaged over a posterior coronal section and one mouse over an anterior coronal section, with silicon probes in the hippocampus. **e**, Same as **b**, showing an illustrative 1-h recording of sleep in a mouse. Color-shaded box indicates sleep epochs. Middle: enlargement of the 5-min box (six periods). Bottom: enlargement of the 50-s box (one period). Please note how LFP beta and CBV cofluctuate with a phase shift and how CBV rises in all brain regions during high beta. **f**, Same as **c** for the mouse experiment. Color-shaded box indicates sleep epochs. In **c** and **f**, the total number of epochs is given in parentheses. **g**, Statistics computed on all 5-min uninterrupted sleep/wake epochs in all four animals for the Pogona experiment. Top: mean autocorrelogram for CBV and LFP during sleep and cross-correlogram during sleep and wake. Bottom left: distribution of the infraslow period in LFP and CBV during sleep, centered on 100 s in all four animals (as indicated by cross signs). Bottom right: comparative distribution of coupling amplitude in sleep and wake (Methods). Please note that the LFP–CBV coupling is significantly stronger in sleep than in wake in all four animals (*$P < 0.05$; **$P < 0.01$; ***$P < 0.001$; rank-sum test). **h**, Same as **g** for the mouse experiment. Statistics computed for all 2-min uninterrupted epochs of NREM, REM sleep and wake in all four animals. Top: note the strong LFP-CBV coupling in all four animals during NREM sleep. Bottom left: the distribution of periods is centered on 50 s (as indicated by cross signs). Bottom right: the LFP–CBV coupling is significantly stronger in NREM sleep than in REM sleep or wake in all animals. nr., number; S, sleep; W, wake; NR, NREM sleep; R, REM sleep.

https://doi.org/10.1038/s41593-025-02159-y

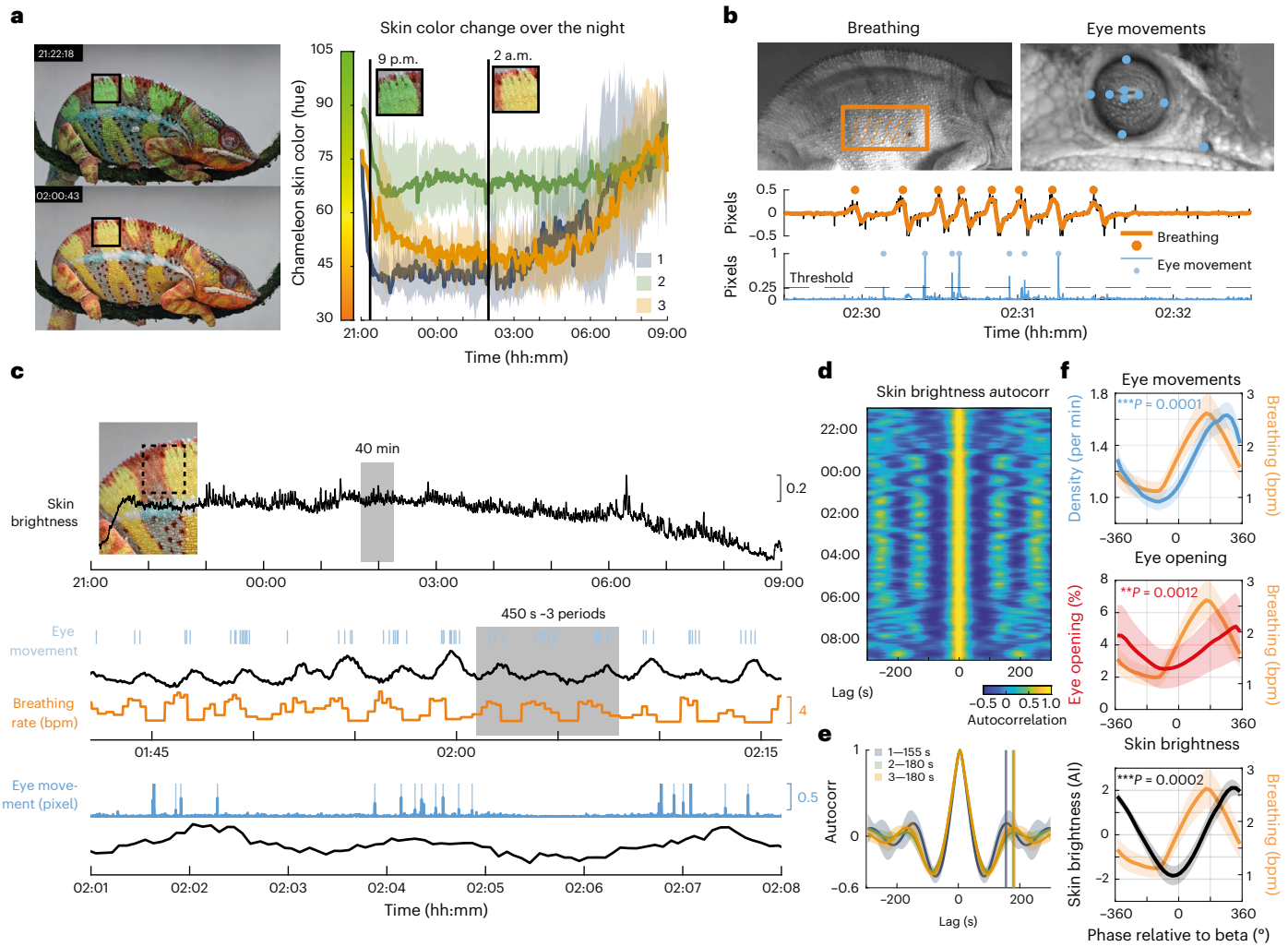

Fig. 4 | Infraslow rhythm in skin brightness coupled with eye movements, eye openings and breathing in sleeping chameleons. a, Left: sleeping chameleon photographed in the darkness (<1 lux) at different times of the night, showing the range of skin colors observed. Right: time series of chameleon skin color hue (insets show two illustrative frames) imaged every 5 s across the nocturnal sleep period for 12 h ($n = 3$). **b**, Top left: breathing extraction using an optical flow algorithm in a stationary ROI (orange rectangle). Top right: eye movement detection using tracked points on the eye and head of the chameleon. Middle: standardized trace of breathing signal (black—raw; orange—smoothed). Bottom: standardized eye movement signal (blue line). **c**, Top: illustrative 12-h recording of skin brightness in an ROI (dashed rectangle) during sleep. Middle: enlargement of the 40-min box showing infraslow rhythmicity in skin brightness (black), breathing rate (bpm; orange) and eye movements (vertical light blue line). Bottom: enlargement of the 450-s box (three periods) showing the raw eye-movement signal (blue) with detected events (blue ticks) and skin brightness (black). The *x* axis indicates the time of day. **d**, Autocorrelation map of the smoothed skin-brightness signal from the same recording shown in **c**, revealing strong periodicity around 150 s. The *x* axis indicates lag; *y* axis indicates time. **e**, Mean autocorrelation of smoothed skin-brightness signals for each animal, with mean skin-brightness periods marked by vertical lines. **f**, Mean values for rate of eye movement (blue eye opening (red) and skin brightness (black) relative to the phase of the breathing (orange lines), computed over all sleep bouts in all three chameleons (shaded boxes—s.e.m.). ROI, region of interest.

coupling during REM sleep and no coupling during wake (Fig. 3e,h and Extended Data Fig. 8; $P < 0.001$). Beta power led CBV signal by only ~3 s, consistent with the time constants of neurovascular coupling in rodents (Fig. 3h and Extended Data Fig. 8). These findings in the bearded dragons and mice reveal similar brain-wide cerebrovascular infraslow rhythms during sleep that are tightly coupled with the neural infraslow rhythms, thus providing strong evidence that reptile infraslow and mouse NREM infraslow rhythms are homologous.

We extended our assessment of sleep-related infraslow activity by taking advantage of several unique characteristics of chameleons, specifically their extreme ocular mobility and changes in skin coloration and brightness. In male panther chameleons, we examined covariation in breathing rate, heart rate, eye movements, skin color (hue) and brightness, as well as DVR beta power during sleep across the night (Fig. 4a,b, Extended Data Fig. 9 and Supplementary Videos 2 and 3). Animals were placed on a stationary hanging branch to ensure a consistent body position across trials, and they remained in the cage for 12 h from 9 p.m. until 9 a.m. in low light (<1 lux) and at a room temperature of 24 ± 1.7 °C (Fig. 4a). We observed slow color changes—from green to yellow—at the beginning of the dark phase and a return to the initial color as the onset of light approached (Fig. 4a and Supplementary Video 2). Skin-color changes, however, showed no clear periodicity across sleep and wake, and they did not vary with breathing rate or eye movements. These changes likely reflect a hormonal mechanism, as in insects or fish, rather than direct muscle control of the chromatophores as in octopuses and cuttlefish[23], which can produce phasic pigmentation changes during sleep[24,25]. Beginning ~1 h into the recording session, skin brightness began to cycle with a period of 175.7 ± 18.3 s (Fig. 4c–e) that was in phase with the infraslow beta rhythm (Extended Data Fig. 9b–j and Supplementary Video 3).

Moreover, clusters of eye movements, which are more frequent and faster than in any other lizard species (Fig. 4c), occurred during high-beta periods and increased heart rate (Extended Data Fig. 9 and Supplementary Video 3); these eye-movement clusters occurred in phase with the increases in skin brightness, which—in these periodic breathers—were usually immediately preceded by the first breath of a bout of three to four breaths (Fig. 4c,f and Extended Data Fig. 9j). These variations in skin brightness may reflect variations in peripheral blood oxygenation, suggesting that infraslow rhythms also reflect changes in the peripheral circulation. Finally, chameleons also tended to open their eyes during high-beta periods (Fig. 4f, Extended Data Fig. 9h–i and Supplementary Video 2), suggesting that these brief periods are microarousals. If so, then the eye movements during these periods likely indicate visual scanning of the environment.

Collectively, these results across seven distant lizard species demonstrate the presence of a conserved sleep-dependent infraslow rhythm that affects brain and body processes and suggest that the infraslow rhythm was first expressed in the common ancestor of this order. Additionally, because our findings in lizards appear similar to those in mammals and birds—after taking temperature-dependent differences into account—they suggest that sleep-related infraslow activity is an ancestral feature of amniotes. In bearded dragons, the association of high-beta DVR activity with occasional bouts of eye movements was interpreted as evidence of a REM-like sleep state[16,19]. Because high-beta periods alternated with low-beta periods rich in high-voltage activity, this second state was proposed to be NREM like[16,19]. An alternative explanation is that the two states correspond to the phases of a single infraslow rhythm, similar to that reported during NREM sleep in mammals[6]. This alternative hypothesis is supported by the current finding that the coupling in bearded dragons between the infraslow beta rhythm and changes in CBV is similar to that in mice during NREM—not REM—sleep. Thus, our findings are inconsistent with the claim that high-beta periods in lizards are indicative of REM sleep having evolved in a common ancestor to lizards, mammals and birds. In addition, in lizards whose body temperature is dependent on ambient temperature, increasing ambient temperature shortens the period of infraslow oscillations without suppressing them[19], which contrasts with what would be expected for REM sleep in mammals[26].

Infraslow rhythms in mammals during NREM sleep are associated with periodic fluctuations in the autonomic system and arousal[6,7,9,10,27] and cerebral vasomotion[13], and it has been proposed that these processes, which also co-occur with pupil dilation in mice[9], reflect microarousals that perhaps serve an antipredator 'sentinel' function. However, demonstrations of periodic skin-color changes and twitching in sleeping cuttlefish[25] and octopuses[24], twitches in apparently asleep spiders[28] and alternating brain states without eye movements in zebrafish[29] or without twitches in lizards underscore both the evolutionary diversity and the convergent features of sleep. Additional studies are needed to test the competing hypotheses about the sub-architecture of sleep. For now, the identification of infraslow rhythms in sleeping lizards opens new comparative avenues for exploring the rhythm's functions and reshapes the continuing discussion surrounding the evolution of sleep states.

Online content

Any methods, additional references, Nature Portfolio reporting summaries, source data, extended data, supplementary information, acknowledgements, peer review information; details of author contributions and competing interests; and statements of data and code availability are available at https://doi.org/10.1038/s41593-025-02159-y.

References

1. Le Bon, O. Relationships between REM and NREM in the NREM-REM sleep cycle: a review on competing concepts. *Sleep. Med.* **70**, 6–16 (2020).
2. Vyazovskiy, V. V. & Tobler, I. The temporal structure of behaviour and sleep homeostasis. *PLoS ONE* **7**, e50677 (2012).
3. Steriade, M., Contreras, D., Curro Dossi, R. & Nunez, A. The slow (< 1 Hz) oscillation in reticular thalamic and thalamocortical neurons: scenario of sleep rhythm generation in interacting thalamic and neocortical networks. *J. Neurosci.* **13**, 3284–3299 (1993).
4. De Gennaro, L. & Ferrara, M. Sleep spindles: an overview. *Sleep. Med. Rev.* **7**, 423–440 (2003).
5. Blumberg, M. S., Lesku, J. A., Libourel, P.-A., Schmidt, M. H. & Rattenborg, N. C. What is REM sleep?. *Curr. Biol.* **30**, R38–R49 (2020).
6. Lecci, S. et al. Coordinated infraslow neural and cardiac oscillations mark fragility and offline periods in mammalian sleep. *Sci. Adv.* **3**, e1602026 (2017).
7. Parrino, L., Ferri, R., Bruni, O. & Terzano, M. G. Cyclic alternating pattern (CAP): the marker of sleep instability. *Sleep. Med. Rev.* **16**, 27–45 (2012).
8. Watson, B. O. Cognitive and physiologic impacts of the infraslow oscillation. *Front. Syst. Neurosci.* **12**, 44 (2018).
9. Yüzgeç, Ö, Prsa, M., Zimmermann, R. & Huber, D. Pupil size coupling to cortical states protects the stability of deep sleep via parasympathetic modulation. *Curr. Biol.* **28**, 392–400 (2018).
10. Osorio-Forero, A. et al. Noradrenergic circuit control of non-REM sleep substates. *Curr. Biol.* **31**, 5009–5023 (2021).
11. Osorio-Forero, A. et al. Infraslow noradrenergic locus coeruleus activity fluctuations are gatekeepers of the NREM–REM sleep cycle. *Nat. Neurosci.* **28**, 84–96 (2025).
12. Kjaerby, C. et al. Memory-enhancing properties of sleep depend on the oscillatory amplitude of norepinephrine. *Nat. Neurosci.* **25**, 1059–1070 (2022).
13. Helakari, H. et al. Human NREM sleep promotes brain-wide vasomotor and respiratory pulsations. *J. Neurosci.* **42**, 2503–2515 (2022).
14. Bueno-Junior, L. S., Ruckstuhl, M. S., Lim, M. M. & Watson, B. O. The temporal structure of REM sleep shows minute-scale fluctuations across brain and body in mice and humans. *Proc. Natl Acad. Sci. USA* **120**, e2213438120 (2023).
15. Libourel, P. A. & Herrel, A. Sleep in amphibians and reptiles: a review and a preliminary analysis of evolutionary patterns. *Biol. Rev. Camb. Philos. Soc.* **91**, 833–866 (2016).
16. Shein-Idelson, M., Ondracek, J. M., Liaw, H.-P., Reiter, S. & Laurent, G. Slow waves, sharp waves, ripples, and REM in sleeping dragons. *Science* **352**, 590–595 (2016).
17. Libourel, P.-A. et al. Partial homologies between sleep states in lizards, mammals, and birds suggest a complex evolution of sleep states in amniotes. *PLoS Biol.* **16**, e2005982 (2018).
18. Norimoto, H. et al. A claustrum in reptiles and its role in slow-wave sleep. *Nature* **578**, 413–418 (2020).
19. Albeck, N., Udi, D. I., Eyal, R., Shvartsman, A. & Shein-Idelson, M. Temperature-robust rapid eye movement and slow wave sleep in the lizard Laudakia vulgaris. *Commun. Biol.* **5**, 1310 (2022).
20. Libourel, P.-A. & Barrillot, B. Is there REM sleep in reptiles? A key question, but still unanswered. *Curr. Opin. Physiol.* **15**, 134–142 (2020).
21. Bergel, A., Deffieux, T., Demené, C., Tanter, M. & Cohen, I. Local hippocampal fast gamma rhythms precede brain-wide hyperemic patterns during spontaneous rodent REM sleep. *Nat. Commun.* **9**, 5364 (2018).
22. Macé, E. et al. Functional ultrasound imaging of the brain. *Nat. Methods* **8**, 662–664 (2011).
23. Figon, F. & Casas, J. in *Encyclopedia of Life Sciences* 1–11 (Wiley, 2018).
24. Medeiros, S. L. et al. Cyclic alternation of quiet and active sleep states in the octopus. *iScience* **24**, 102223 (2021).

25. Iglesias, T. L., Boal, J. G., Frank, M. G., Zeil, J. & Hanlon, R. T. Cyclic nature of the REM sleep-like state in the cuttlefish *Sepia officinalis*. *J. Exp. Biol.* **222**, jeb174862 (2019).
26. Parmeggiani, P. L. REM sleep related increase in brain temperature: a physiologic problem. *Arch. Ital. Biol.* **145**, 13–21 (2007).
27. Halász, P., Terzano, M., Parrino, L. & Bódizs, R. The nature of arousal in sleep. *J. Sleep. Res.* **13**, 1–23 (2004).
28. Rößler, D. C. et al. Regularly occurring bouts of retinal movements suggest an REM sleep–like state in jumping spiders. *Proc. Natl Acad. Sci. USA* **119**, e2204754119 (2022).
29. Leung, L. C. et al. Neural signatures of sleep in zebrafish. *Nature* **571**, 198–204 (2019).

Methods

Ethics and permits

All animal experiments were conducted in accordance with the 3R principles in animal experimentation and the European Community Council Directive for the use of research animals (2010/63/EEC). The protocols and procedures for lizards and rats were approved by the local ethics committee for animal experimentation of the University of Lyon 1, the National Museum of Natural History, ESPCI Paris and by the Ministry of Education and Research (APAFIS114005-2017092010302481 v5, APAFIS 21756-2019082014201741 v4 and APAFIS 38797-2022092916416349 v5). The pigeon experiments were conducted in accordance with German animal welfare guidelines and were approved by the local ethics committees for animal experimentation (Government of Upper Bavaria, permit ROB-55.1-2532.Vet_02-18-89).

The human sleep data are based on a prospective, observational, longitudinal study, 'Sleep and Cognitive Functioning,' conducted at the Inselspital, Bern University Hospital (Switzerland). The protocol was approved by the Institutional Review Board of Inselspital (4893) and the Ethics Committee of the Canton of Bern (KEK 2021-000726) and was conducted in accordance with the Declaration of Helsinki and Good Clinical Practice guidelines. The study originally recruited participants to examine sleep and cognitive function; however, all participants provided separate informed consent for the reuse of their anonymized data.

Animals and participants

Lizards. All lizards used in the study were purchased from official local dealers and were adults at the time of testing. For the electrophysiological recordings, we used four bearded dragons (*P. vitticeps*; female = 2 and male = 2; weight = 290–412 g), three Egyptian starred agamas (*Laudakia vulgaris*; female = 3; weight = 117 ± 20 g), three Sudan plated lizards (*B. major*; male = 3; weight = 114–138 g), three tokay geckos (*G. gecko*; female = 2 and male = 1; weight = 74–78 g), one panther chameleon, (*F. pardalis*; male = 1; weight = 192 g), two leopard geckos (*E. macularius*; male = 2; weight = 72 g) and three Argentine tegus (*S. merianae*; female = 1 and male = 2; weight = 2,200–3,300 g). For the functional ultrasound recordings, an additional four bearded dragons (male = 2 and female = 2; weight = 315–438 g) were used. An additional three panther chameleons (male = 3; weight = 150–200 g) were used for behavioral recordings only.

Rats and mice. Five Sprague Dawley brown rats (males, age >3 months; weight = 350–590 g) were included. Four C57Bl6 mice (males; weight = 32.8–35.1 g) were also used for the functional ultrasound experiment.

The information mentioned above is summarized in Supplementary Table 1.

Humans. Data from eight healthy human participants (Eastern Cooperative Oncology Group grade of 0–1) without sleep pathology (female = 6 and male = 2; mean age = 44.6 ± 16.3 years, range = 21–73 years) were analyzed. The following exclusion criteria were applied: known (that is, self-reported or documented in medical records) pre-existing structural deformations of the brain (for example, previous stroke, traumatic brain injury, neuroinfection and tumors), known progressive neurological diseases, known psychiatric diseases, concomitant benzodiazepine medication, drug or alcohol abuse, inability to follow study procedure and pregnancy.

Pigeons. Eleven adult domestic pigeons (female = 5 and males = 6; weight = 241.5 ± 13.4 g) were used. Birds were reared and housed in enriched colony aviaries as described in ref. 30.

Surgery

Brain atlas for lizards. In the absence of suitable brain atlases for lizards and to target specific brain regions, structural magnetic resonance imaging (MRI) and computed tomography (CT) scans were performed on at least one individual from each species. Before the surgery, animals were sedated at half the usual surgical dose injected intramuscularly (ketamine = 50 mg kg^{-1}; medetomidine = 100 µg kg−1). After anesthesia induction, they were secured in a stereotaxic apparatus (Bruker Animal Handling Systems). MRI acquisitions were performed in vivo using a 7T Bruker BioSpec MRI system (Bruker Biospin MRI GmbH) equipped with a set of gradients of 440 mT m^{-1} and controlled using the Bruker ParaVision 5.1 workstation. A Bruker birdcage volume coil (inner diameter = 72 mm and outer diameter = 112 mm) was used for signal transmission, and a Bruker single-loop surface coil (25 mm diameter) was used for signal reception, positioned on the head of the animal to target the brain. High-resolution axial MRI images were obtained using a 3D T2-weighted fat-saturated image based on rapid acquisition with the relaxation-enhanced method. The acquisition parameters were as follows: effective echo time (TE) = 41.34 ms, repetition time (TR) = 2,000 ms, rapid acquisition with the relaxation-enhanced factor = 8, number of average = 1 and bandwidth = 75 kHz. The region of interest (brain) was acquired under a field of view of 3 × 1.5 × 3 cm and a matrix size of 386 × 192 × 128 pixels, providing an in-plane resolution of 78 × 78 × 156 µm and a resolution of 78 $µm^3$ after zero-filling interpolation. The total acquisition time for each animal was approximately 1 h.

CT acquisitions were performed using an INVEON system (Siemens) with a tension of 80 kV, a current of 500 µA, an exposure time of 900 ms with 720 steps and a low magnification. The reconstruction of the final volume enables us to obtain a voxel size of 55.62 $µm^3$. The total acquisition time was about 45 min.

After imaging, animals were injected intramuscularly with atipamezol (200 µg kg^{-1}) to reverse the effects of medetomidine. The MRI and CT scans were aligned together using at least ten common points to create specific brain atlases for each species with Aviso 7.0 (VSG)[17]. The coordinates of the electrode placement were determined based on the merged images[17].

To locate the electrode positions in vivo, some individuals underwent additional CT scans at the end of the experiments[17]. The subsequent images were realigned to the previously obtained MRI and CT scans. Electrode position was inferred based on the electrode locations indicated in the second CT scan[17]. When electrode positions were checked, they were located in the anterior part of the telencephalon (anterior or posterior DVR) as expected, validating the precision of our surgical procedure. After the experiments, the implants and the electrodes fell off after 6–12 months. Once fully healed and after a veterinary checkup, the animals were adopted as pets.

Electrophysiology. *Lizards*. Once the implantation coordinates were determined for each animal, the lizards underwent surgery. Surgical anesthesia was achieved using a mixture of ketamine (100 mg kg^{-1}) and medetomidine (200 µg kg^{-1}) injected intramuscularly[31]. Reflexes and respiratory rate were checked throughout the surgery to ensure adequate anesthesia. During the surgery, two stainless steel electrodes were implanted bilaterally in the intercostal muscles to measure heart rate, and two were implanted in the neck muscles to assess muscle tone. The animals were then secured in a stereotaxic apparatus. One screw was implanted on top of each eye on the medial part of the supraorbital ridge. Two bundles of four to eight tungsten electrodes (35 µm diameter; spaced 200–500 µm apart) were implanted bilaterally in the DVR. The implantation coordinates were defined based on the stereotaxic atlas targeting the DVR using a skull ref. 17, usually the pineal eye, which was untouched during the surgery to avoid impacting thermoregulation or circadian rhythms. Each bundle of electrodes was implanted at species-specific depths in the DVR, determined from MRI and CT scans—leopard gecko (1.5–3.5 mm from the skull), tokay gecko (1–2.5 mm), Sudan plated lizard (2.5–4.5 mm), Argentine tegu (5–7 mm), panther chameleon (4.4–6.8 mm), Egyptian rock agama (2–5 mm) and bearded dragon (2–4 mm). Two electrooculogram (EOG) electrodes

(gold-plated stainless steel), two electromyogram (EMG) electrodes (stainless steel, bent 3–4 mm at the tip to form a hook, with the coating removed at the tip) and two electrocardiogram (ECG) electrodes (stainless steel, attached subcutaneously on each side of the chest) were implanted. One screw, inserted on the most caudal part of the parietal bone, served as a reference. All wires were then connected to a head connector (EIB-36-PTB Neuralynx) or a custom-made electrode interface board, which was secured to the skull using Superbond (Sun Medical). Dental Paladur cement (Heraeus Kuzler) was applied around the head connector to protect the wires and connector. At the end of the surgery, the animals were injected intramuscularly with atipamezol (400 µg kg^{-1}) and subcutaneously with an anti-inflammatory solution (carprofen 1 mg kg^{-1}) mixed with a glucose solution (5%).

Rats. In rats, anesthesia was induced by inhalation of 3% isoflurane in oxygen and was maintained with 1.5% isoflurane at 1 l m^{-1}. A prior injection of carprofen (5 mg kg^{-1}) was administered subcutaneously to prevent pain. A thermal probe was inserted into the rectum, and body temperature was maintained at 37 °C using a heating blanket. After shaving, cleaning and disinfecting the skin above the skull, a 3 cm midline incision was made, and the cranial bone was exposed and cleaned. An electrode for EOG recording (a gold-plated ball, 1 mm in diameter and connected to a multistrand cable) was placed under each eyelid, and then the cable was tunneled under the skin of the skull to the incision area. The rats were placed on their backs. To measure respiratory activity ($n = 1$), two electrodes (a gold-plated ball, 1 mm in diameter) connected to a multistrand cable were sutured to the diaphragm (after incision of the abdominal skin and creating a 4-cm opening of the abdominal muscle to access the diaphragm); the cables were tunneled under the skin to the incision area of the skull. After suturing the abdominal incision with absorbable thread, the rats were placed in a stereotaxic apparatus (David Kopf Instruments). Then, electrodes for measuring EEG activity were placed bilaterally above the olfactory bulb, frontal cortex, parietal cortex and cerebellum. The EEG electrodes consisted of a stainless-steel screw connected by solder to a multistrand cable. Screws were fixed to the skull after making holes of 0.8 mm in diameter using a dental drill. The two electrodes placed above the cerebellum served as references for the EEG signals. The EEG screws were secured to the skull with a light-curing glue. Two EMG electrodes (a gold-plated ball, 1 mm in diameter) connected to a multistrand cable were inserted into the neck muscles. Finally, two ECG electrodes (gold-plated balls, 1 mm in diameter) were positioned bilaterally in the intercostal area, secured with sutures and tunneled to the incision area of the skull.

Pigeons. Pigeons were surgically instrumented for recording EEG activity from both hemispheres and neck EMG under isoflurane anesthesia (1–3% in 0.5 l m^{-1} oxygen). The birds were administered an injection of diazepam (2 mg kg^{-1}) into the breast muscle 15 min before surgery, an injection of metamizole (150 mg kg^{-1}) into the breast muscle shortly before isoflurane anesthesia, four drops of procaine (2%) for local analgesia before skin incision, an intramuscular injection of meloxicam (0.5 mg kg^{-1}) and lidocaine gel to the wound at the end of the surgical procedure. The electrodes consisted of round-tipped gold pins (0.5 mm diameter) for the EEG and gold-plated electrode balls (1 mm diameter) for the EMG. The EEG electrodes were placed over the visual hyperpallium, which is visible through a window of thin bone on the surface of the cranium. Two EEG electrodes were placed on the dura overlying the left and right hyperpallium (2.5 and 3 mm lateral to the midline for the anterior and posterior electrodes, respectively, and separated by 5–6 mm along the anterior–posterior axis). One EEG reference electrode was placed above the cerebellum. The EMG electrodes were inserted into the muscles of the neck.

Functional ultrasound imaging. *Bearded dragons*. After weighing, the bearded dragons were deeply anesthetized by intramuscular injection of ketamine (100 mg kg^{-1}) and medetomidine (200 µg g^{-1}). The top of the skull was cleaned with an iodine solution followed by 70% alcohol. The bearded dragon was then placed in a stereotaxic apparatus. Ophthalmic ointment (liposic) was applied to the eyes to prevent drying. The scales of the skull above the imaging plane were removed with a scalpel. Four holes were drilled (two at the front and two at the back of the skull) into which screws were inserted to serve as a reference and ground for the electrophysiological recordings. A window was then drawn over the area to be imaged, and the overlying bone was carefully cut out with a drill without affecting the dura mater. Four additional holes were then drilled using stereotaxic coordinates based on the MRI and CT scans. The dura mater was resected before implanting the tungsten microelectrode bundle (four wires, 35 µm in diameter) bilaterally in the telencephalon. Microthermistors were inserted to measure brain temperature. Two hook-shaped stainless-steel EMG electrodes were sutured into the neck muscles. Gold-plated microelectrodes were placed under the eyelids to measure ocular activity. A 125-µm-thick polymethyl-pentene (TPX) sheet (Goodfellow) was cut to the size of the cranial window, disinfected with alcohol and dried. This material has a tissue-like acoustic impedance that allows for the undistorted propagation of ultrasound waves at the acoustic gel-prosthesis and prosthesis–saline interfaces. It was positioned above the exposed brain and sealed with dental cement (GC Unifast TRAD). Diluted (1/10) betadine was then applied around the skin to prevent infection. All electrodes were connected to an implant that was fixed to the skull using dental cement. At the end of the surgical procedure, the bearded dragons were injected intramuscularly with atipamezol (400 µg kg^{-1}) and subcutaneously with a mixture of an anti-inflammatory (carprofen 1 mg kg^{-1}) mixed in a glucose solution (5%), and were allowed to recover for 2 days. Each bearded dragon was equipped with a permanent connector and a movable protective cap (13 mm long, 1.4 mm wide, 5 mm high and a total mass of approximately 0.5 g).

Mice. After weighing, the mouse was deeply anesthetized using isoflurane (3.0%) and maintained through a mask (1.5%). Analgesia was performed via subcutaneous injection of buprenorphine (0.05 mg kg^{-1}) and subcutaneous injection of lidocaine (4 mg kg^{-1}). The top of the skull was cleaned with an iodine solution (betadine gel). The animal was then placed in a stereotaxic apparatus. Ophthalmic ointment (liposic) was applied to the eyes to prevent drying. A parasagittal incision was performed to expose the skull. Two holes were drilled above the cerebellum into which screws were inserted to serve as a reference and ground for the electrophysiological recordings. A window was drawn over the area to be imaged and the overlying bone was carefully removed using a drill without affecting the dura mater. One additional hole was drilled following stereotaxic coordinates (anteroposterior = 2.3 mm, mediolateral = 1.6 mm). The dura mater was resected before implanting a silicon probe (Cambridge Neurotech) mounted on a movable nanodrive (Cambridge Neurotech) into the dorsal hippocampus. A 125-µm-thick TPX sheet (Goodfellow) was cut to the size of the cranial window, disinfected with alcohol and dried; it was positioned above the exposed brain and sealed with dental cement (GC Unifast TRAD). Diluted (1/10) betadine was applied around the skin to prevent infection. The implant was fixed to the skull using dental cement. At the end of the surgical procedure, the mice were injected intraperitoneally with a glucose solution (5%) for fluid replacement and allowed a 7-day recovery period. Each mouse was equipped with a custom permanent connector and a movable protective cap (13 mm long, 3 mm wide, 5 mm high and a total mass of approximately 0.5 g).

Data acquisition

Electrophysiological recordings. *Lizards*. All the lizards were maintained individually in a glass terrarium adapted to their size and lifestyle. They were fed vegetables (for bearded dragons) daily, crickets, mealworms or dead mice (depending on their diet) thrice weekly. Water was provided ad libitum. Animals were maintained under a 12-h light/12-h dark cycle, and room temperature was maintained around

25 °C. A precise temperature measure was provided continuously using a thermistor attached to the skull implant. Each terrarium contained a shelter transparent to infrared light, except for the chameleon, which was recorded on a branch available in the terrarium. Two infrared (850 nm) panels were set on top of the terrarium and were always on. The Argentine tegu's data were reused from ref. 17; refer to this publication for recording conditions.

Electrophysiological signals were recorded using custom-made wireless recording devices[32] (Manitty SAS). The signals were recorded at 256 Hz with a hardware low-pass filter set at 100 Hz and a high-pass filter at 0.1 Hz. The total weight of the device, including the battery, was 6–11 g. This configuration allowed constant unthethered recording for more than 48 h. Signals were acquired using a custom Matlab script (Matlab r2016b, MathWorks), and the videos were synchronized with an output TTL to trigger the beginning and ending of each video. The animals were able to move freely and appeared undisturbed by the weight of the equipment.

Rats. After 10 days of recovery postsurgery, rats were placed in a Plexiglas barrel (40 cm in diameter) with bedding, enrichment, food and water. Barrels were placed inside an electrically shielded recording chamber. Environmental housing conditions were maintained at stable levels (humidity and ventilation), with an air temperature of 23±1°C and a 12-h light/12-h dark cycle (lights on at 7:00 a.m.). Two of the five rats were recorded using a tethered system. The cable from the skull was attached to a rotating connector (Bilaney, Plastics One) that allowed movement during recording. Rats were acclimated to the recording chamber and cable for at least three consecutive days. Briefly, signals were amplified (EEG = 2,000×, others = 5,000×; A-M systems, Model 3500), filtered (bandpass 1–100 Hz for the EEG and 10–100 Hz for the others), digitized (NI USB 6343 card; National Instrument; sampling rate 1,024 Hz) and acquired using Sleepscore software (Viewpoint). The other three rats were recorded using the same wireless system (Manitty SAS) as that used for the lizards, using the same protocol as described previously[32]. For all rats, each EEG signal was referenced to the cerebellar EEG electrode, and muscle tone, eye movements and cardiac and respiratory activity were assessed using a differential signal[33]. The data were collected at 256 Hz for at least 48 h.

Humans. Participants were recorded in a single room at the hospital. The lights were switched off when the patient wished, and the data were collected overnight. Nocturnal sleep recordings were conducted either with a 256-channel EEG coupled with polysomnography (high-density EEG (hd-EEG); Geodesic EEG System, Physiobox; Magstim EGI) or clinical eight-electrode polysomnography (PSG; SOMNO HD, Somnomedics; Embla N700, Natus) according to the protocol of the Department of Neurology of the Inselspital Bern. The choice of the assessment (that is, hd-EEG or clinical polysomnography) was based on the willingness of the participant to undergo a study-specific hd-EEG assessment. ECG, EMG, EOG and breathing parameters were recorded according to the clinical protocol of Inselspital Bern.

Pigeons. The pigeon recordings were collected as described previously[30]. During the recording phase, the animals were housed individually in an indoor enriched aviary (1 m × 2 m × 2 m; 12-h light/12-h dark photoperiod; air temperature, 21 °C) adjacent to, and in visual and auditory contact with, two other pigeons that were housed in similar aviaries. Food and water were provided ad libitum. After at least 1 week of postsurgical recovery, the pigeons were progressively habituated to the recording equipment. The birds were then recorded during the 12-h night while confined to their preferred elevated sleeping perch[30].

Functional ultrasound imaging. *Bearded dragons*. Data were acquired in three sessions. Surgery was performed on the first day, followed by a 2-day recovery period and a 3–8-day observation period. Animal 1 was prepared for sagittal recordings, whereas animals 2–4 were prepared for coronal (Extended Data Fig. 8). All lizards were maintained individually in a glass terrarium and were fed vegetables daily. Water was provided ad libitum. Animals were maintained under a 12-h light/12-h dark cycle, and the room temperature was constant and set at around 25 °C. Air temperature was measured continuously with a thermistor fixed to the electrophysiological device on the head. Each terrarium was transparent to infrared light. Two infrared (850 nm) panels were set on top of the terrarium and were always on.

Mice. Data were acquired in two sessions. Surgery was performed on the first day, followed by a 7-day recovery period and a 3–7-day postoperative recording period. Mice were housed individually and maintained under a 12-h light/12-h dark cycle, with a constant room temperature of approximately 25 °C. Water and food were provided ad libitum. Mice were recorded between 9 am and 6 pm, with the majority of recordings occurring between 9 a.m. and 2 p.m.

Functional ultrasound images are Power Doppler images obtained via the ultrafast compound Doppler imaging technique[22]. The ultrasonic probe (Vermon) is a linear array made of 64 (mice and bearded dragons) or 128 (bearded dragons) transducers working at a 15-MHz central frequency (spatial pitch = 0.11 mm; transducer element = 2.000 × 0.110 mm^2; bandwidth = 46% at −6 dB, corresponding to 11–18 MHz). Image resolution is 0.110 × 0.110 mm^2. The probe has an acoustic lens with an elevation focal distance of 8 mm and an elevation focal width of 400 µm, corresponding to the thickness of the imaging plane. A 150-cm cable length and 12-g probe weight ensured relative freedom and comfort for the animal. Penetration of the ultrasound waves across 20 mm of brain tissue allowed us to image a full section of the lizard brain (Fig. 3a) and mouse brain (Fig. 3d). Compound plane-wave frames were obtained by a coherent summation of beamformed complex in phase/quadrature (IQ) images obtained from the sonification of the medium with a set of successive plane waves with specific tilting angles. Given the tradeoff between frame rate, resolution and imaging speed, a plane-wave compounding method using ten 2°-apart angles of sonification (from −5° to +5°) was chosen. As a result, the pulse repetition frequency of the plane-wave transmissions was 500 Hz.

Each vascular image CBV was acquired at 1 Hz for the bearded dragons and 2 Hz for the mice, with a 400 ms sonification period and a pause of 600 ms for the bearded dragons and 100 ms for the mice. This strategy ensured continuous acquisition of imaging without dropping frames or saturating memory for prolonged time periods (1–8 h for the bearded dragons and 1–2 h for the mice). To build the images of CBV from the raw back-scattered echoes, radiofrequency signals were delayed and summed to form IQ matrices through a process known as beamforming. These matrices were then decomposed via singular value decomposition to separate slow/global movements due to pulsatility and tissue motion from fast/local movements caused by echogenic particles crossing a voxel during a full cardiac cycle. The first 60 components were removed, which optimally exploited the spatiotemporal dynamics of the full Doppler film for clutter rejection[34]. Notably, power Doppler images were computed by taking the power of the full Doppler spectrum, including a range of speeds in large and small vessels, with an inferior bound of 5–10 mm s^{-1} in axial velocity[35], thus giving a signal proportional to the number of echogenic particles that have crossed a single voxel during 400 ms (with a sufficient axial velocity).

Behavioral experiment with chameleons. Before their normal nocturnal sleep period, the chameleons were transferred to a transparent glass cage. They were placed on a thin, stationary hanging branch. Chameleons remained in the cage illuminated with a dim white light measured at less than 1 lux at the chameleon's position for a period of 12 h from 9 p.m. until 9 a.m. the following morning, after which they were transferred to their home habitat with ad libitum food and water.

Video recordings lasted throughout the night. For the three chameleons studied, 18–25 nights were recorded. The three best sessions for each chameleon, based on video quality and animal position, were fully processed. The first trials were not analyzed because the animals were not habituated to the environment and tended to move on the branch during the first hours of the evening session.

Video recording. For all lizards, the behavior of the animals was monitored using multiple cameras (Dragonfly2 and DR2-HIBW, Point Gray) equipped with a bandpass filter in the near-infrared wavelength. One or two cameras recorded the full area, and one or two were dedicated to the animal shelter. The videos were recorded at 15 Hz, 24 h a day (VPCore2 (Viewpoint) or StreamPix (Norpix)). The chameleon, equipped for electrophysiological recording, was also equipped with two head-mounted minicamera modules (NanEye, ams AG; 1 mm × 1 mm) for two nights, connected to an image-processing board (BAP Image Systems GmbH, AC62KUSB) for recording eye movements at 10 frames per second.

For the behavioral experiments with chameleons, each trial was recorded using color and infrared video. Color video was recorded using a Nikon Z6 camera. An image was acquired every 5 s with a 4-s exposure time (ISO 8000, F5.6; noise reduction off, HDR off and D-lighting off; white balance calibrated using white paper). The camera was positioned to capture a side view of the animal. Images were stored directly to the computer (DigiCamControl). One infrared FLIR BlackFly GigE camera was placed alongside for recording at 10 frames per second. A second infrared camera was occasionally used to record the other side of the animal or to obtain a front view of it. All cameras stored images to a computer using custom scripts in MATLAB that added a precise timestamp. The cage was illuminated using two diffuser lights, producing a measured interior of 1 lux. The infrared video permitted visualization of higher-frequency phenomena, such as breathing rate, body twitching and eye movements. The 4-s-long exposure color imaging allowed for accurate skin-color data acquisition.

Data analysis

Sleep identification and scoring. Sleep and wakefulness in the lizards were scored based on the animal behavior. An animal was considered sleeping if its head was lying on its support (floor, branch or wall of the terrarium) for at least 30 min, usually with the eyes closed (except for the tokay geckos that do not have mobile eyelids). Rare, short eye-opening periods (<5 s) were not rejected from the sleep period. Every other behavior was considered as wake. For the functional ultrasound experiment, when behavior was briefly not available (due to missing video), we detected movement from the accelerometer. Human sleep was scored according to the American Academy of Sleep Medicine criteria (2020, v2.6). In birds, rats and mice, periods were scored as NREM sleep, REM sleep and wake using previously published criteria[30,33].

Sleep segmentation. For lizards, all behavioral sleep periods were included in the analysis; in rats and birds, only NREM was included; and in humans, only N2 was included. Because in rats and pigeons, bouts of REM sleep are very brief—often shorter than one or two periods of the infraslow rhythm (~50 s on average)—it was not meaningful to compute infraslow periods during these bouts. This was particularly the case as we used a 3-min sliding window for *z*-score normalization in all species for comparative purposes. Every period of sleep was divided into 1-h bouts when possible. The minimal bout duration included for lizards was 15 min and 5 min for the endotherms. Beta/sigma power, heart rate, breathing rate, eye movements and muscle tone were extracted from the data for each bout.

LFP and EEG recording. For the lizards, the LFP channel with the highest signal-to-noise ratio was selected for analysis. The Sudan plated lizards were unique in that some LFP channels exhibited a 1–2 s burst of 20-Hz activity every time they breathed. We did not analyze data from these channels, as the breathing burst falls within the beta band (10–30 Hz), which we used to quantify the infraslow rhythm. For rats, we used EEG data from either the frontal or parietal electrodes, depending on the signal-to-noise ratio of the data. For mice, the LFP channel was chosen as the one closest to the pyramidal layer in the CA1 region of the hippocampus, detected based on maximum ripple frequency (150–250 Hz) during NREM sleep using previously published methods[36]. For humans, we mostly used the central electrode (C4) referenced to the contralateral mastoid. In birds, we used a hyperpallial electrode. To extract the sigma and beta power in the LFP and EEG, we first filtered the signal within the band of interest (beta = 10–30 Hz; sigma = 10–15 Hz), then computed the instant power using the squared absolute value of the Hilbert transform and then smoothed the signal using a 10-s sliding window average.

Heart rate. Heart rate was extracted by detecting peaks in the ECG record. Filtering (high or low pass) and thresholding were applied to each recording. The function 'findpeaks' in MATLAB was used. Instantaneous heart rate was computed from the interval between peaks and smoothed using a 20-s sliding-window average. The quality of the heartbeat detection was visually checked for every sleep bout by generating Supplementary Fig. 2.

Breathing rate. A custom Python 3.9 script using the optical flow algorithm (OpenCV and MATLAB) was used to measure breathing rate from infrared video. Small regions of interest on the animal's abdomen that showed the greatest respiratory movements were analyzed. The algorithm calculated the average frame-by-frame pixel change in the form of a magnitude and angle vector. For each frame of the video, the image timestamp, pixel-region magnitude and pixel-region angle were saved. When viewed as a time series, region-specific pixel changes across time indicate breathing movements. As with heart rate, filtering, thresholding and smoothing were adjusted for each recording. Breathing rate was extracted from the interval between each breath, and the data were smoothed using a 5-s sliding-window average. The thresholding was adapted for each recording. The quality of breath detection was visually checked for every sleep bout by generating Supplementary Fig. 2.

Eye movements. As with heart and breathing rates, eye movement density was computed by detecting eye movements and smoothing the interval between eye movements using a 20-s sliding-window average from the EOG recording. A 1-Hz high-pass filter and a 10-Hz low-pass filter were used. The thresholding was adapted for each recording. The output of this analysis was visually checked for every sleep bout by generating Supplementary Fig. 2.

For the chameleons experiment, eye movements were quantified using DeepLabCut[37] from the infrared video. To train the system to recognize eye movements, we labeled by hand four points around the chameleon's eyelid, four points on the outer eye socket and two additional points on the nose and mouth (Fig. 4b). Each model's training dataset consisted of 40–60 randomly selected frames. For each trial, a cropped region of the infrared video containing only the eye and surrounding features was labeled and trained for 60,000–100,000 epochs using a ResNet-101 convolutional neural network. Once trained, all frames for the entire video were analyzed, and the corresponding tracked points were exported in tabular format. Each point was measured as an (x,y) pixel coordinate position within the frame. The tracked points were then synchronized with the matching frame timestamps. Further processing was done in MATLAB (R2021a). The duration of time that the chameleon's eyes were open or closed was quantified using the pixel distance between the top and bottom eyelid points. To quantify a steady eye movement signal robust to noise caused by brief

imperfections in point tracking with DeepLabCut, we tracked four separate points on the chameleon's eyelid. For each frame, we measured the pixel distance traveled by each point between consecutive frames and used the aggregate minimum of these four distances. When the eye movement signal surpassed a threshold, the event was considered an eye movement. The thresholds for detecting eye opening and eye movements were based on pixel distance and were adjusted depending on the proximity of the camera to the subject and the resolution of the eye.

Muscle tone. To derive a measure of muscle tone, the EMG signal was high-pass filtered using a Butterworth filter with a cutoff frequency of 10 Hz and an order of 10. Then, the squared absolute value of the Hilbert transform was computed and smoothed using a 10-s sliding-window average.

Body temperature. Because lizards lack internal heat production, air temperature serves as a proxy for body temperature; this is not the case for mammals and birds, which produce heat internally and regulate their body temperature independently of air temperature. In lizards, air temperature was measured using a thermistor attached to the head-mounted electrophysiological device. Temperature was measured continuously during the session. In the rats, humans and pigeons, which are endothermic, mean body temperatures were estimated from known values for these species (rats, 37.5 °C (ref. 38); humans, 36.8 °C (ref. 39); pigeons, 38.9 °C (ref. 40)).

Chameleon skin brightness and hue values. Chameleon skin color and brightness changes were acquired by selecting and tracking two separate color regions on the chameleon. The colored band was used to estimate the color change (Fig. 4a), and the red interband was used to measure the brightness (Fig. 4c). At the center of each selected region, a 10–30-pixel radius circle measured the average hue and brightness of all interior pixels. This color measurement was done in the hue, saturation and value digital color representation with the following integer value ranges: $H = 0–179$; $S = 0–255$; $V = 0–255$. For every frame of the video, the hue, saturation and value components were extracted and saved.

CBV. CBV was measured using functional ultrasound in bearded dragons and mice; simultaneously, LFPs were recorded from the DVR of bearded dragons and the hippocampus of mice. To derive CBV values from the raw Power Doppler videos in bearded dragons and mice, we performed voxel-wise normalization with reference to a 3-min baseline sleep period. For each voxel in the image, we computed the average value on this baseline period and subsequently subtracted this mean value and divided it by the mean of the raw Doppler movie. This process is analogous to computing $\Delta F/F$ signals in fluorescence microscopy and provides normalization and rescaling of ultrasound data, yielding a measure in terms of percent of variation relative to baseline (CBV% change). As no brain atlas was available for the bearded dragon, we registered a representative ultrasound image into the 3D MRI volume acquired for each animal to derive global and regional CBV signals in regions of interest. For mice, we manually registered the brain images using coronal sections of the Allen Brain Atlas[41].

Ultrasound frames were segmented into ten regions of interest. Regional CBV temporal series were obtained by averaging the time series of all individual voxels in the corresponding region of interest. For accurate measures, this process requires that the probe be fixed on the animal's head, which we ensured using precision screws. Regional and global CBV time series were smoothed using a 20-s Gaussian smoothing kernel for bearded dragons and a 10-s kernel for mice. To account for any potential drift in the CBV signals and LFP signals during the recording sessions, we normalized each time series by z scoring using a sliding window of 5 min for bearded dragons and 2 min for mice. Our final datasets consisted of Doppler videos sampled at one to two images per second for recording durations lasting 1–8 h.

Calculating infraslow periods. For the LFP (lizards) and EEG (rats, humans and pigeons) data for each sleep bout, infraslow periods were measured by computing autocorrelations. To do this, a sliding autocorrelation (Figs. 1e and 4d, Extended Data Fig. 3 and Supplementary Figs. 1 and 3–12) was computed from the beta power signal (10–30 Hz) and z scored using a 3-min sliding window. We used the 10–30 Hz frequency band, as the phenomenon is broadband (Extended Data Figs. 2 and 3), and this band had already been used in other studies on the bearded dragon. The data were $z$scored over 3-min sliding windows to compensate for amplitude changes across time, trials and species. We also provide an analysis using different window sizes in Supplementary Fig. 1, showing that the infraslow oscillation becomes independent of sliding-window length above 2–3 min. Autocorrelations were computed using a 1-s step over a 300-s window with a maximum lag of 300 s. The autocorrelations were then normalized for each window based on the value at zero lag. The first negative (half period) and positive peaks of the autocorrelation, along with their corresponding lags (Fig. 1f,g, Extended Data Fig. 3 and Supplementary Figs. 1 and 3–12), were extracted by detecting the first lowest and highest peaks, respectively, with a positive lag and a minimal prominence of 0.05. To demonstrate that the infraslow rhythm is not an artifact of the windowing process, we additionally computed the autocorrelation of the beta band after shuffling the cerebral signal into 5-s segments, repeated 100 times. This analysis showed that the infraslow rhythm was no longer present in the shuffled data (autocorrelation amplitude <0.1 in lizards and <0.15 in endotherms; Supplementary Fig. 1). Autocorrelations of the CBV and LFP signals from the functional ultrasound experiments (Fig. 3b,e and Extended Data Figs. 7 and 8) were computed using a 5-min sliding window in bearded dragons and a 2-min sliding window in mice from the z-scored (detrended) data. The autocorrelation was computed with a 5-s step over a 300-s moving window with a maximum lag of 300 s in bearded dragons and a 150-s moving window with a maximum lag of 150 s in mice, for each uninterrupted NREM sleep, REM sleep or wake epoch (minimal duration 300 s in bearded dragons and 100 s in mice). The mean autocorrelation functions (Fig. 3b,e,g,h and Extended Data Figs. 7 and 8) were computed by averaging the corresponding autocorrelation functions obtained on each sleep epoch.

Calculating the physiological variations relative to the cerebral infraslow. To evaluate the variations of physiological parameters (heart rate, breathing rate, muscle tone and eye movement density) relative to the cerebral infraslow rhythm, we averaged the physiological signals on the phase of the beta power 10–30 Hz (Figs. 2 and 4 and Supplementary Figs. 3–12). The reference signal (for example, beta power) was first normalized using a 3-min z-scored sliding window and then smoothed using a 10-s sliding window average. The phase was extracted from the Hilbert transform computed on the normalized signal. The phase was then linearly interpolated between $-\pi$ and π. For each physiological signal (heart rate, breathing rate, muscle tone and eye movements), the values were discretized along 30, $\pi/15$-width bins according to the phase of the reference signal. The mean value for each phase bin was then computed for each sleep bout. For discrete values (eye movements or breathing), the percentage of events occurring within each phase bin was computed (Supplementary Figs. 3–12). The main vector length and the phase-locking value were then evaluated according to ref. 42 by computing the mean vector in Cartesian coordinates (Extended Data Fig. 9).

Coupling between CBV and LFP. The coupling between the CBV and the beta power was estimated by calculating the cross-correlation between the normalized beta power and the normalized CBV. The cross-correlation was computed with a 5-s step over a 300-s

moving window with a maximum lag of 300 s in bearded dragons and a 150-s moving window with a maximum lag of 150 s in mice. The cross-correlation peaks (coupling amplitude) were detected as the closest local maximum around 0 with a minimal prominence of 0.05. The mean cross-correlation functions (Fig. 3b,e,g,h) were computed by averaging the corresponding cross-correlation functions obtained on each sleep/wake epoch. The first negative (half period) and positive peak of the autocorrelation and the corresponding lag (Fig. 3b,e and Extended Data Figs. 7 and 8) were extracted by detecting the first lowest and highest peak, with a positive lag, with a minimal prominence of 0.05.

Statistics

No statistical methods were used to predetermine sample sizes, but our sample sizes are similar to those reported in similar previous publication[16,17]. Only sleep bouts that were too short were excluded from the analysis. However, no animals were excluded. All the statistics were computed using MATLAB. The differences between the phases (Fig. 2c and Extended Data Fig. 3) were assessed using a two-sided Wilcoxon signed-rank test. A Bonferroni correction was used to adjust for multiple comparisons (Extended Data Fig. 3). The α was set to 0.05 for all tests. ($^{*}P < 0.05$, $^{**}P < 0.001$, $^{***}P < 0.0001$). Phase-locking statistics (Fig. 4f and Extended Data Fig. 9) were computed by testing the uniformity of the circular distribution using the Rayleigh test[43]. Differences in coupling amplitude (Fig. 3g,h) were computed using the rank-sum test under the null hypothesis that differences are driven by the same distribution ($^{*}P < 0.05$, $^{**}P < 0.001$, $^{***}P < 0.0001$). Unless otherwise noted, data are expressed as mean ± s.e.m.

Reporting summary

Further information on research design is available in the Nature Portfolio Reporting Summary linked to this article.

Data availability

The datasets used in this study are part of an ongoing research project, and additional analyses are currently being conducted. For this reason, the raw data are not yet publicly available but can be shared upon request.

Code availability

Shared upon request.

References

30. Ungurean, G., Martinez-Gonzalez, D., Massot, B., Libourel, P.-A. & Rattenborg, N. C. Pupillary behavior during wakefulness, non-REM sleep, and REM sleep in birds is opposite that of mammals. *Curr. Biol.* **31**, 5370–5376 (2021).
31. Barrillot, B. et al. Intramuscular administration of ketamine-medetomidine assures stable anaesthesia needed for long-term surgery in the Argentine tegu *Salvator merianae*. *J. Zoo. Wildl. Med.* **49**, 291–296 (2018).
32. Massot, B. et al. ONEIROS, a new miniature standalone device for recording sleep electrophysiology, physiology, temperatures and behavior in the lab and field. *J. Neurosci. Methods* **316**, 103–116 (2019).
33. Libourel, P.-A., Corneyllie, A., Luppi, P.-H., Chouvet, G. & Gervasoni, D. Unsupervised online classifier in sleep scoring for sleep deprivation studies. *Sleep* **38**, 815–828 (2015).
34. Demené, C. et al. Spatiotemporal clutter filtering of ultrafast ultrasound data highly increases Doppler and fUltrasound sensitivity. *IEEE Trans. Med. Imaging* **34**, 2271–2285 (2015).
35. Mace, E. et al. Functional ultrasound imaging of the brain: theory and basic principles. *IEEE Trans. Ultrason. Ferroelectr. Freq. Control* **60**, 492–506 (2013).
36. Liu, A. A. et al. A consensus statement on detection of hippocampal sharp wave ripples and differentiation from other fast oscillations. *Nat. Commun.* **13**, 6000 (2022).
37. Mathis, A. et al. DeepLabCut: markerless pose estimation of user-defined body parts with deep learning. *Nat. Neurosci.* **21**, 1281–1289 (2018).
38. Gudjonsson, S. V. The body temperature in rats on normal and deficient diets. *J. Physiol.* **74**, 73–80 (1932).
39. Geneva, I. I., Cuzzo, B., Fazili, T. & Javaid, W. Normal body temperature: a systematic review. *Open Forum Infect. Dis.* **6**, ofz032 (2019).
40. Phillips, N. H. & Berger, R. J. Regulation of body temperature, metabolic rate, and sleep in fasting pigeons diurnally infused with glucose or saline. *J. Comp. Physiol. B* **161**, 311–318 (1991).
41. Trotts, I., Mikula, S. & Jones, E. G. Interactive visualization of multiresolution image stacks in 3D. *Neuroimage* **35**, 1038–1043 (2007).
42. Hülsemann, M. J., Naumann, E. & Rasch, B. Quantification of phase-amplitude coupling in neuronal oscillations: comparison of phase-locking value, mean vector length, modulation index, and generalized-linear-modeling-cross-frequency-coupling. *Front. Neurosci.* **13**, 573 (2019).
43. Berens, P. CircStat: a MATLAB toolbox for circular statistics. *J. Stat. Softw.* **31**, 1–21 (2009).

Acknowledgements

We would like to thank O. Antonini, from Bebesaurus, for providing materials and valuable advice on the animals' care. We also appreciate the support of the Zoo Parc de la tête d'or and all the zoo keepers and staff who took care of our animals when the animal facility was closed. We are grateful to I. Achin for assistance with data collection, and to C. Bouillot and R. Bolbos from CERMEP for enabling us to acquire high-quality CT scans and MRIs. We also thank P. Tissier for his help with the design of the ultrasound probe holder and K. Homolkova for her help in acquiring functional ultrasound data in mice. We would like to thank A. Peyrache at the Montreal Neurological Institute and Hospital, McGill University, for his assistance with computational resources. The study was funded by the Interdisciplinary mission of the CNRS (PEPS EXOMOD PHYLOREM to P.-A.L.), the French Society for Sleep Research and Medicine (SFRMS to P.-A.L. and B.B.), Rhône-Alpes Institute of Complex Sciences (IXXI, project AMPHISLEEP to P.-A.L.), Max Planck Society (to N.C.R.), National Institutes of Health (R37-HD081168 and R01-HD104616 to M.S.B.), European Sleep Foundation (to M.H.S.), Swiss National Science Foundation (to M.H.S.), AXA Research Fund under the chair New hopes in medical imaging with ultrasound (to A.B.). This project has also received funding from the European Union's Horizon 2020 research and innovation programme under the Marie Skłodowska-Curie grant agreement No 101023337 (A.B.). Chameleons were purchased using funds provided by M.S.B., M.H.S. and N.C.R.

Author contributions

P.-A.L. conceived, designed and supervised the project. A.B. and M.T. built and set up the functional ultrasound experiments. A.B., C.F., B.B. and P.-A.L. conducted the functional ultrasound experiment. A.B. verified and analyzed the functional ultrasound data. B.B., S.A., L. A., A.C. and P.-A.L. conducted the lizard electrophysiology experiments. L.A. and A.C. habituated and cared for the animals. P.-A.L., B.B. and C.C. analyzed the electrophysiological data. G.U. collected the bird data. M.H.S. and I.F. collected the human data. P.-A.L. collected the chameleon data. J.M.S. and P.-A.L. analyzed the chameleon data. B.M. and P.-A.L. conceived the electrophysiological instrumentation. A.B., J.M.S. and P.-A.L. prepared the figures. P.-A.L. wrote the first version of the paper. A.B., A.H., J.M.S., M.S.B., M.H.S., N.C.R. and P.-A.L. reviewed and completed the paper. A.B., A.H., B.B., J.M.S., M.S.B., M.H.S., N.C.R. and P.-A.L. discussed and interpreted the results.

Competing interests
The authors declare no competing interests.

Additional information
Extended data is available for this paper at https://doi.org/10.1038/s41593-025-02159-y.

Supplementary information The online version contains supplementary material available at https://doi.org/10.1038/s41593-025-02159-y.

Correspondence and requests for materials should be addressed to Paul-Antoine Libourel.

Peer review information *Nature Neuroscience* thanks Anita Lüthi, Philippe Mourrain and Vladyslav Vyazovskiy for their contribution to the peer review of this work.

https://doi.org/10.1038/s41593-025-02159-y

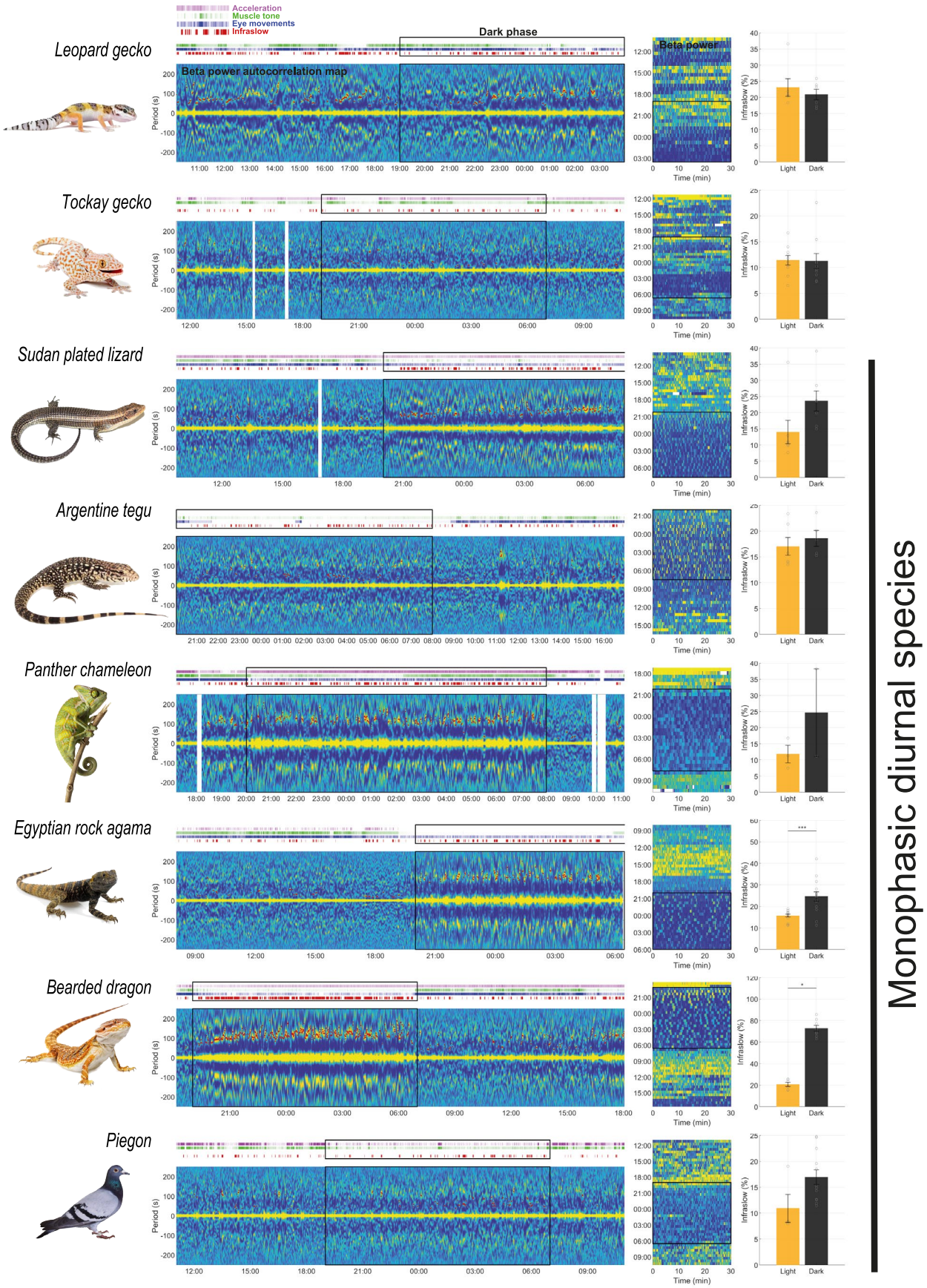

Extended Data Fig. 1 | See next page for caption.

https://doi.org/10.1038/s41593-025-02159-y

Extended Data Fig. 1 | The infraslow rhythms (high autocorrelation) of the beta power are sleep dependent. Each line represents the autocorrelation map of the beta power computed over 24 h for every species. Each red dot shows the highest peak autocorrelation amplitude (higher than the mean of the autocorrelation peaks over 24 h), reflecting the stronger infraslow rhythm. The black rectangle indicates the dark phase. Above the autocorrelation map, the level of activity is represented in pink, the muscle tone is represented in green and the eye movement density in blue. On the right, the color-coded map shows the evolution of the beta power among 30-min windows. High-beta power is coded in yellow, and low-beta power is coded in blue. On the right, the percentage of time (mean value ± s.e.m.) occupied by infraslow rhythms relative to the duration of the dark and light phase shows a predominance of infraslow during the dark period for nocturnal animals. The number of individuals and nights (replicates) per species is indicated in Supplementary Table 1 (row 'number of individual' and 'total number of nights'). The gray circles represent each night (replicates) from all individuals per species. We compared the light and dark phases using a two-sided Wilcoxon signed-rank test (*P<0.05, ***P<0.0001).

https://doi.org/10.1038/s41593-025-02159-y

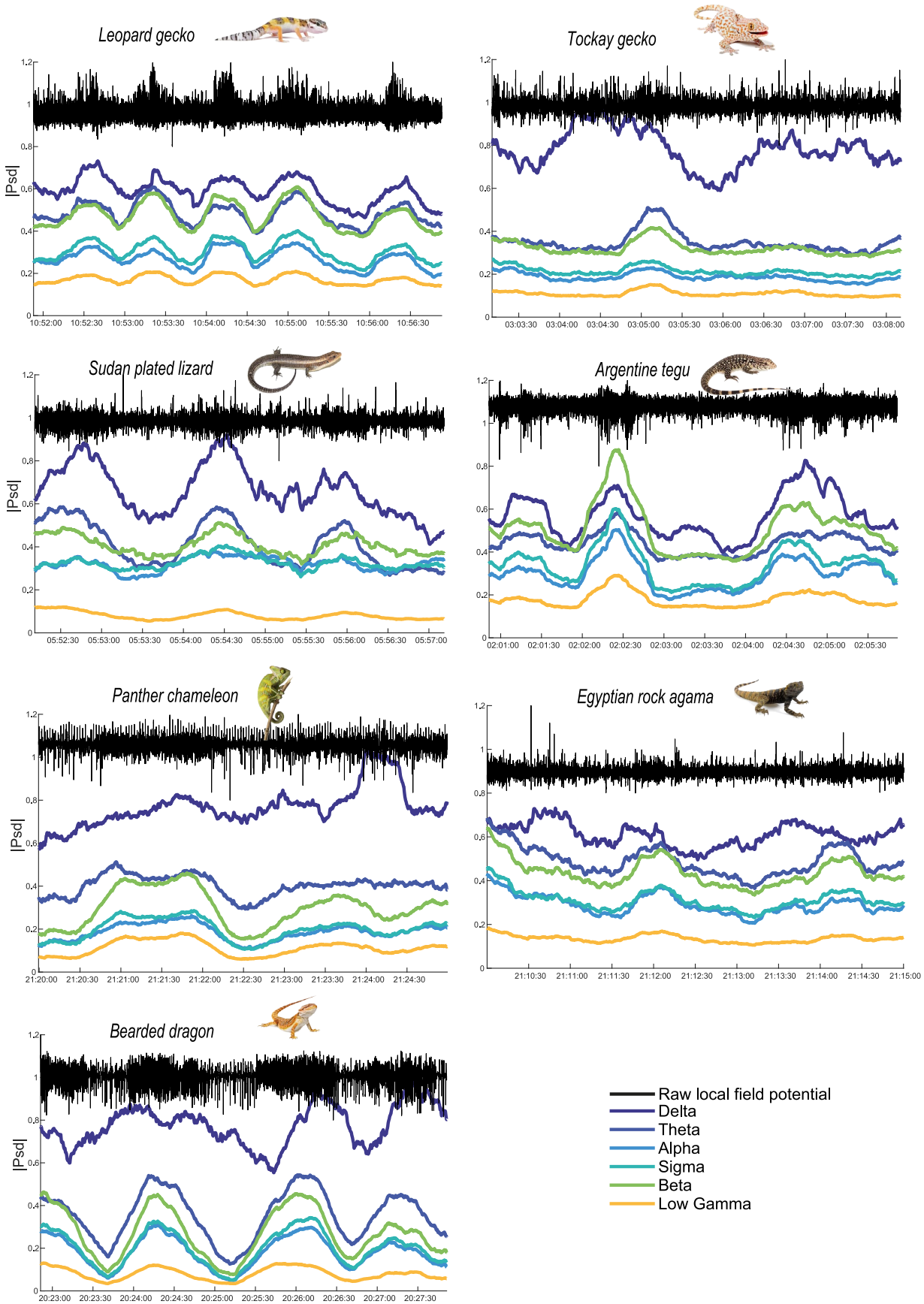

Extended Data Fig. 2 | Spectral band powers fluctuate similarly during sleep in lizards. Each subpanel shows 5 min of cerebral signal during sleep in lizards (black traces). Below, color-coded lines represent the normalized spectral power for the following bands: delta (0.5–4 Hz), theta (4–9 Hz), alpha (9–12 Hz), sigma (10–15 Hz), beta (10–30 Hz) and low gamma (30–40 Hz). The spectral powers are smoothed with a 30-s window sliding average and normalized over the power between 0.5 and 40 Hz.

https://doi.org/10.1038/s41593-025-02159-y

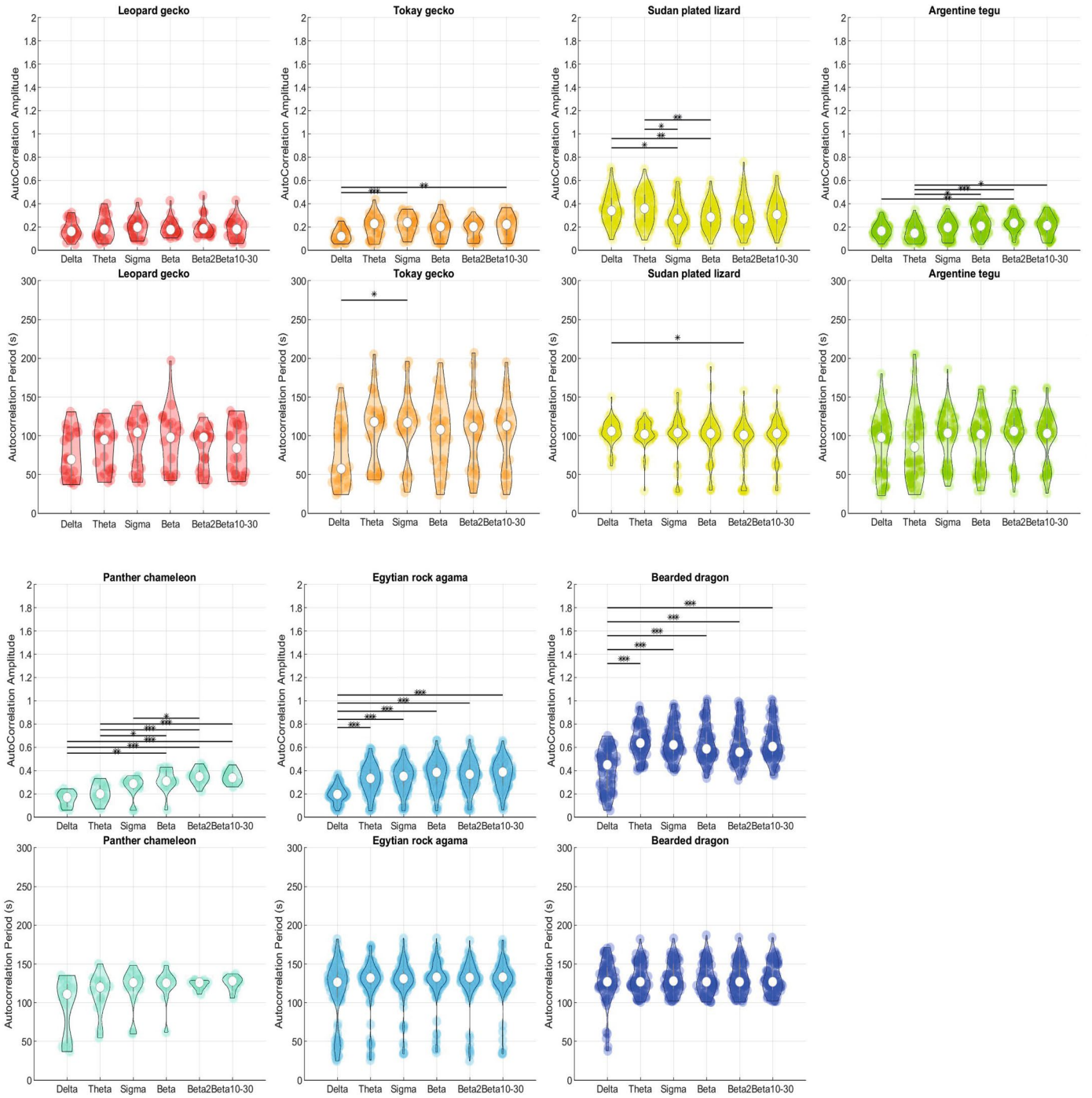

Extended Data Fig. 3 | The infraslow rhythm is a broadband phenomenon. For each lizard species, we computed the lag (period) and the amplitude of the autocorrelation of the brain signal in the delta (1–4 Hz), theta (4–10 Hz), sigma (10–15 Hz), low-beta (15–25 Hz), high-beta (25–40 Hz) and beta (10–30 Hz) bands. We then compared the values of lag and amplitude across species using two-tailed t tests after Gaussian normalization, with a Bonferroni correction applied as a post hoc test. The number of individuals and replicates (sleep bouts) per species is indicated in Supplementary Table 1 (row 'LFP/EEG'). The number of individuals and replicates (sleep bouts) per species is indicated in Supplementary Table 1 (row 'LFP/EEG'). White dots indicate median value across all sleep bouts, color dots indicate all sleep bouts from all individuals and the gray vertical line indicates notch values (*P<0.05, **P<0.001, ***P<0.0001).

https://doi.org/10.1038/s41593-025-02159-y

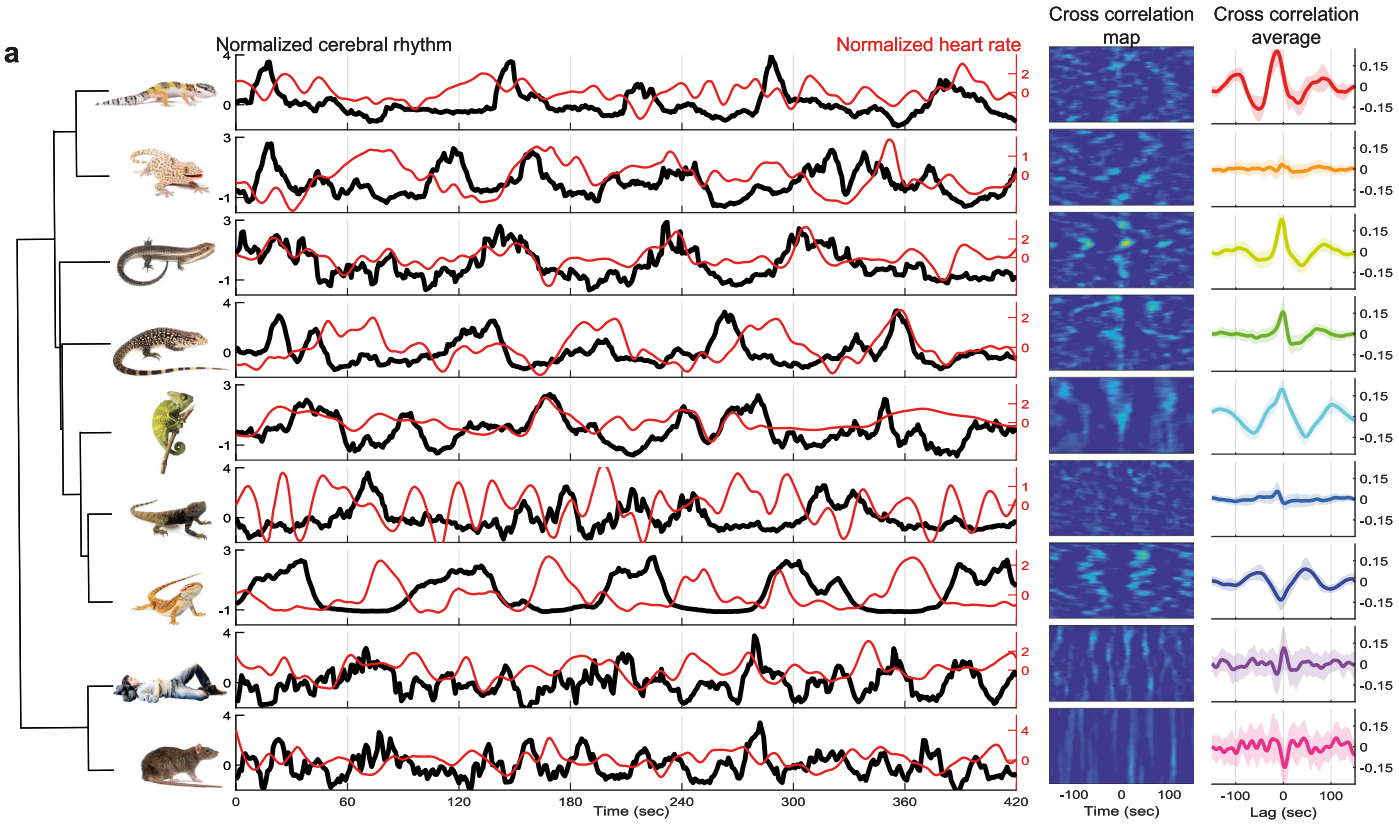

Extended Data Fig. 4 | Coupling between heart rate and beta infraslow rhythm. For each species, the black lines show beta power and heart rate (both z-scored over 10-min sliding windows) across 7 min. On the right, the cross-correlation maps between beta power and heart rate during sleep (NREM and N2 in mammals). The last graph illustrates the averaged ±s.e.m. cross-correlation over all analyzed periods and individuals per species. The figure shows a positive cross-correlation between the beta power and the heart rate in all species except in the bearded dragon and the rat, where the correlation is negative.

https://doi.org/10.1038/s41593-025-02159-y

Bearded Dragon

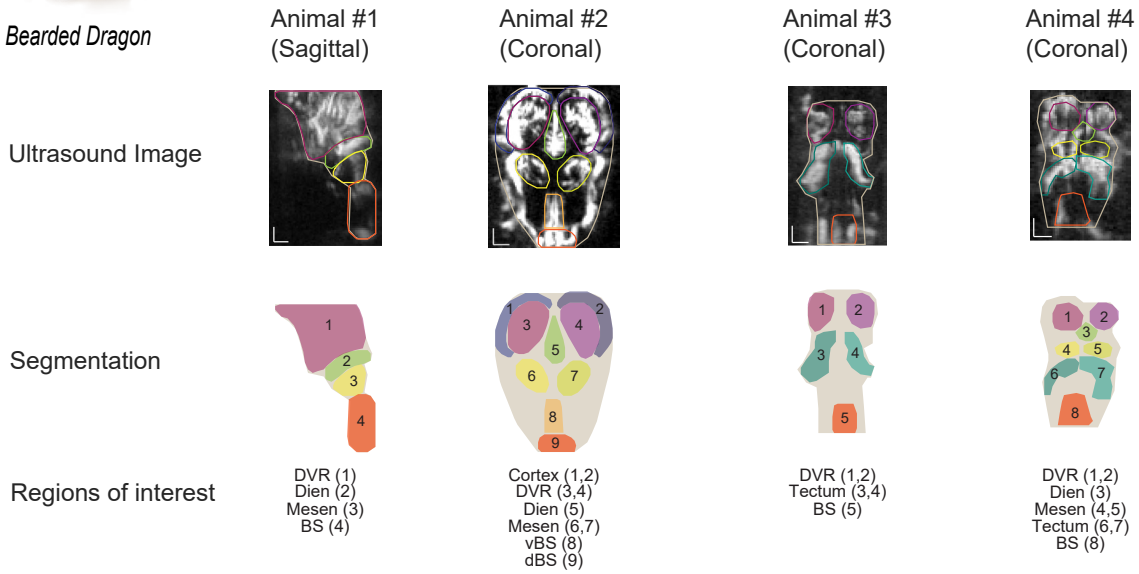

Extended Data Fig. 5 | Overview of the different fields of view for the four different bearded dragons in the functional ultrasound imaging experiment. Example ultrasound image (top), segmentation based on MRI/CT atlas registration (middle) and corresponding regions of interest (bottom) (the grey region representing the whole brain). Animal 1 was prepared for sagittal recordings, while animals 2–4 were prepared for coronal recordings.

https://doi.org/10.1038/s41593-025-02159-y

Bearded Dragon

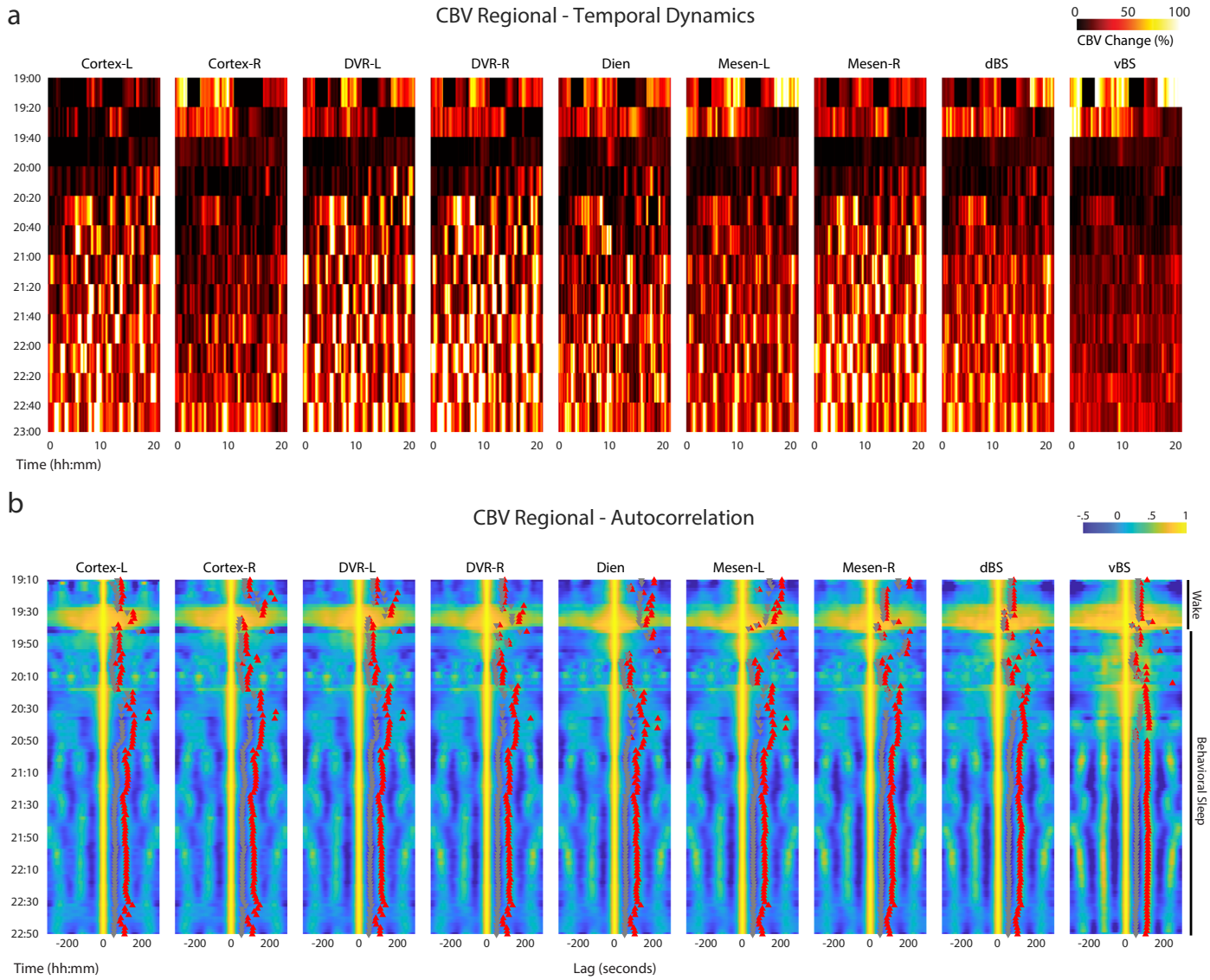

Extended Data Fig. 6 | Regional hemodynamics during a transition from wake to sleep in the bearded dragon. a, Regional CBV dynamics in the nine regions of interest displayed in Extended Data Fig. 5 (Animal #2) (left cortex, right cortex, left DVR, right DVR, diencephalon, left mesencephalon, right mesencephalon, dorsal and ventral brainstem). **b**, Autocorrelation of regional CBV time series computed over 20-min periods with a 2-min sliding window. First positive peak (autocorrelation period) and first negative peaks (autocorrelation half period) are displayed in red and gray, respectively. Note the gradual stabilization of the autocorrelation period toward 100 s in all nine regions of interest.

https://doi.org/10.1038/s41593-025-02159-y

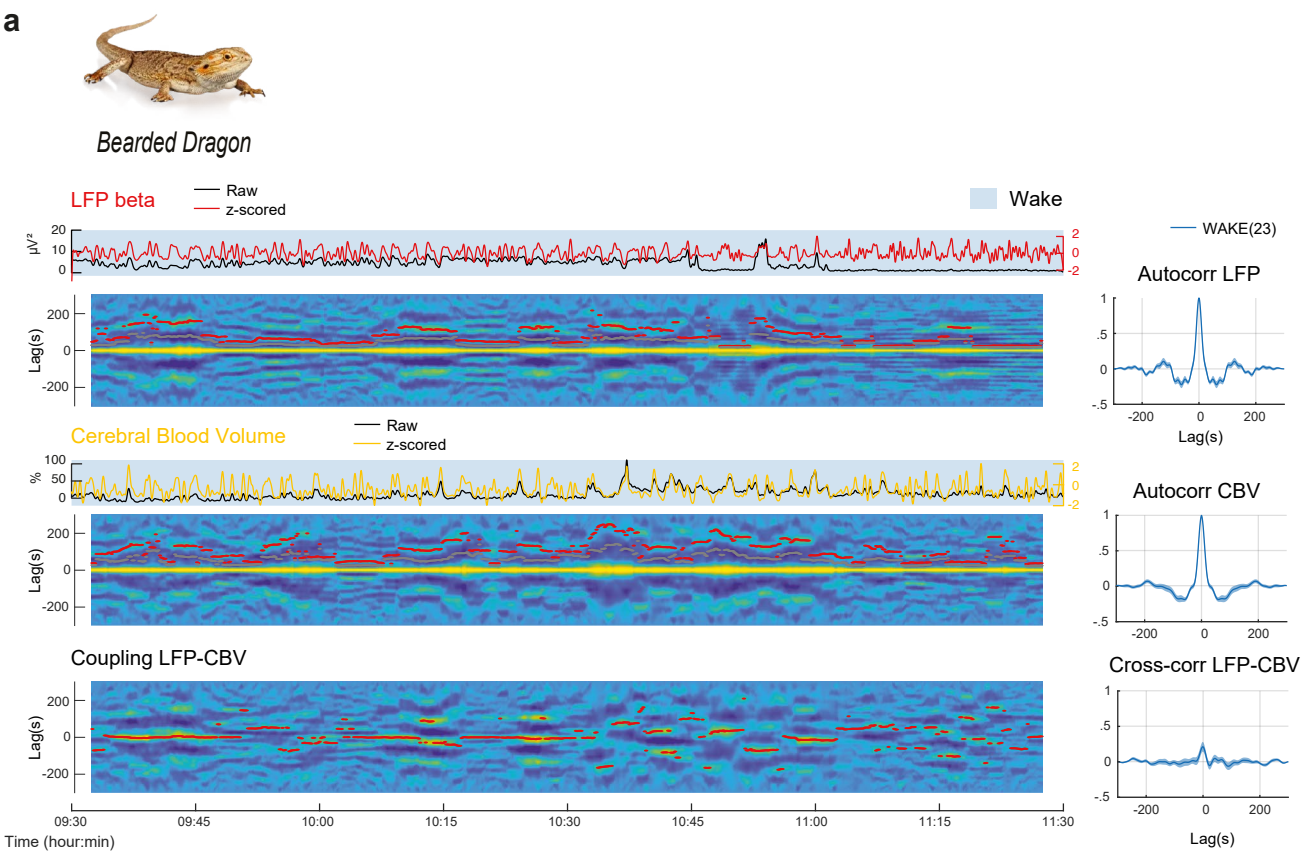

Extended Data Fig. 7 | See next page for caption.

https://doi.org/10.1038/s41593-025-02159-y

Extended Data Fig. 7 | Infraslow rhythms are specific to sleep. a, Same as Fig. 3b,c for a wake recording in the bearded dragon. Top, LFP power in the beta band in the DVR before (black) and after (red) detrending, and the autocorrelation maps computed over a 2-min sliding window. First positive (red) and negative (gray) peaks are displayed. Right, mean auto-correlogram. Middle, same as top, for the mean cerebral blood volume of the whole brain. The absence of strong positive peaks in both auto-correlograms reveals the absence of infraslow rhythm in wake. Bottom, cross-correlogram between LFP and CBV data with the mean cross-correlation function on the right. The low cross-correlation values reveal a low coupling during wake. **b**, Same as Fig. 3e,f for a wake recording in the mouse. Top, LFP power in the beta band (10–30 Hz) in the DVR before (black) and after (red) detrending, and the autocorrelation maps computed over a 5 min sliding window. First positive (red) and negative (gray) peaks are displayed. Right, mean auto-correlogram. Middle, same as top, for the mean cerebral blood volume of the whole brain. The absence of strong positive peaks in both autocorrelograms reveals the absence of infraslow rhythms in wake. Bottom, cross-correlogram between LFP and CBV data with the mean cross-correlation function on the right. The low cross-correlation values reveal a low coupling during wake, with a reinstatement of high values during NREM sleep.

https://doi.org/10.1038/s41593-025-02159-y

Bearded Dragon

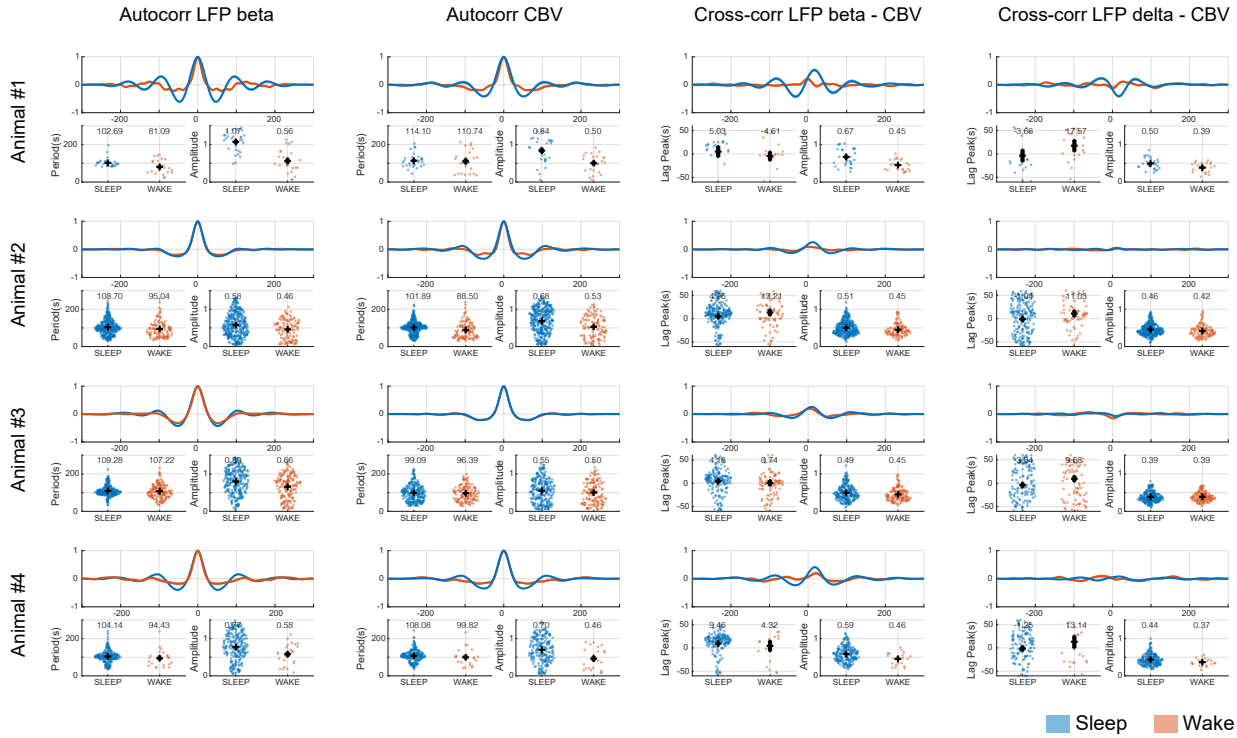

Mouse

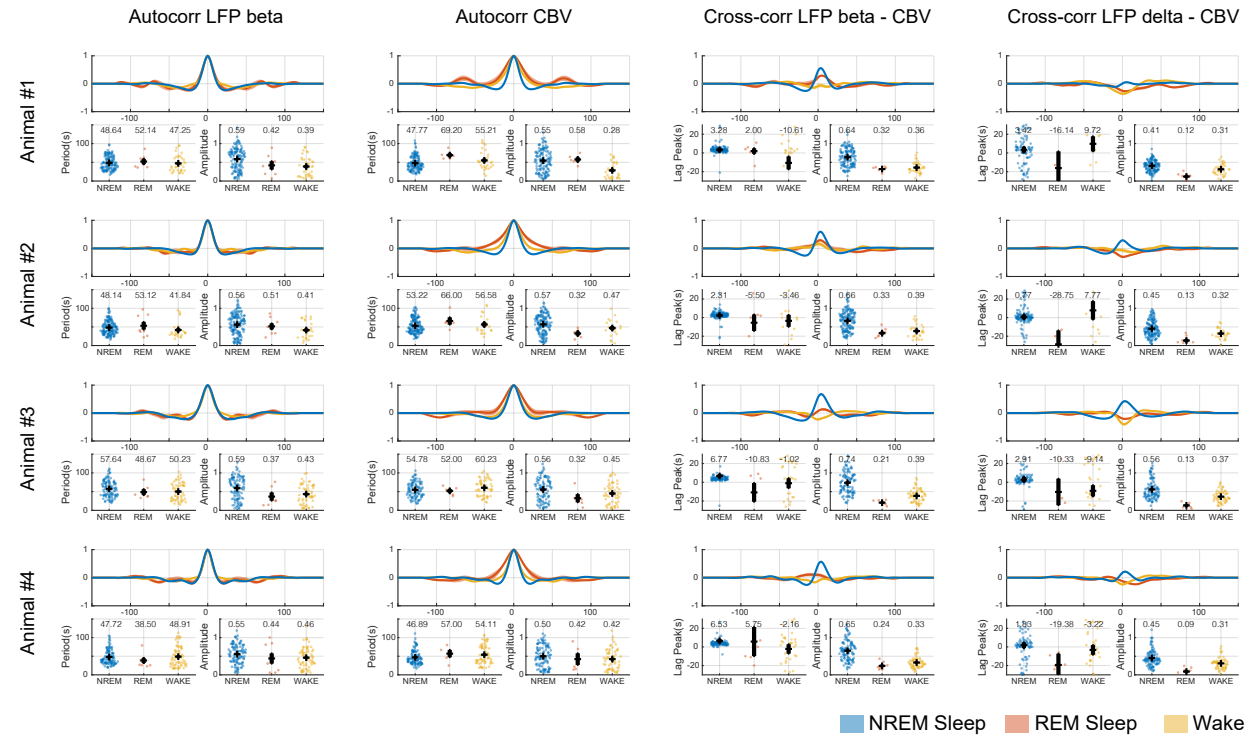

Extended Data Fig. 8 | See next page for caption.

https://doi.org/10.1038/s41593-025-02159-y

Extended Data Fig. 8 | Infraslow rhythms are visible in all animals and are band-specific in bearded dragons and mice. Top (bearded dragon), each row represents an animal. The two left columns display the autocorrelation function for the LFP signal filtered in the beta band (left) and for the CBV signal of the whole brain (middle left). The two right columns display the cross-correlation between the LFP signal filtered in the beta (middle right) or delta (right) bands and CBV. Data are displayed for all 5-min uninterrupted sleep and wake epochs. The distributions of the periods and amplitude of all autocorrelation functions and the x value of the positive peak (lag peak) and amplitude for all cross-correlation functions are displayed below the correlograms. Horizontal black bar—mean. Vertical black bar—mean ± s.e.m. n = 4 animals. Number of wake/sleep bouts per animal—animal 1, n = 23/29; animal 2, n = 115/347; animal 3, n = 156/268; animal 4, n = 23/231. Bottom (mouse): same as top with statistics computed on all 2-min uninterrupted wake, NREM and REM sleep bouts. n = 4 animals. Number of wake/NREM sleep/REM sleep bouts per animal—animal 1, n = 36/7/132; animal 2, n = 25/8/151; animal 3, n = 53/6/105; animal 4, n = 66/8/109. All autocorrelation or cross-correlation functions are displayed below the correlograms. Horizontal black bar—mean. Vertical black bar—mean ± s.e.m.

https://doi.org/10.1038/s41593-025-02159-y

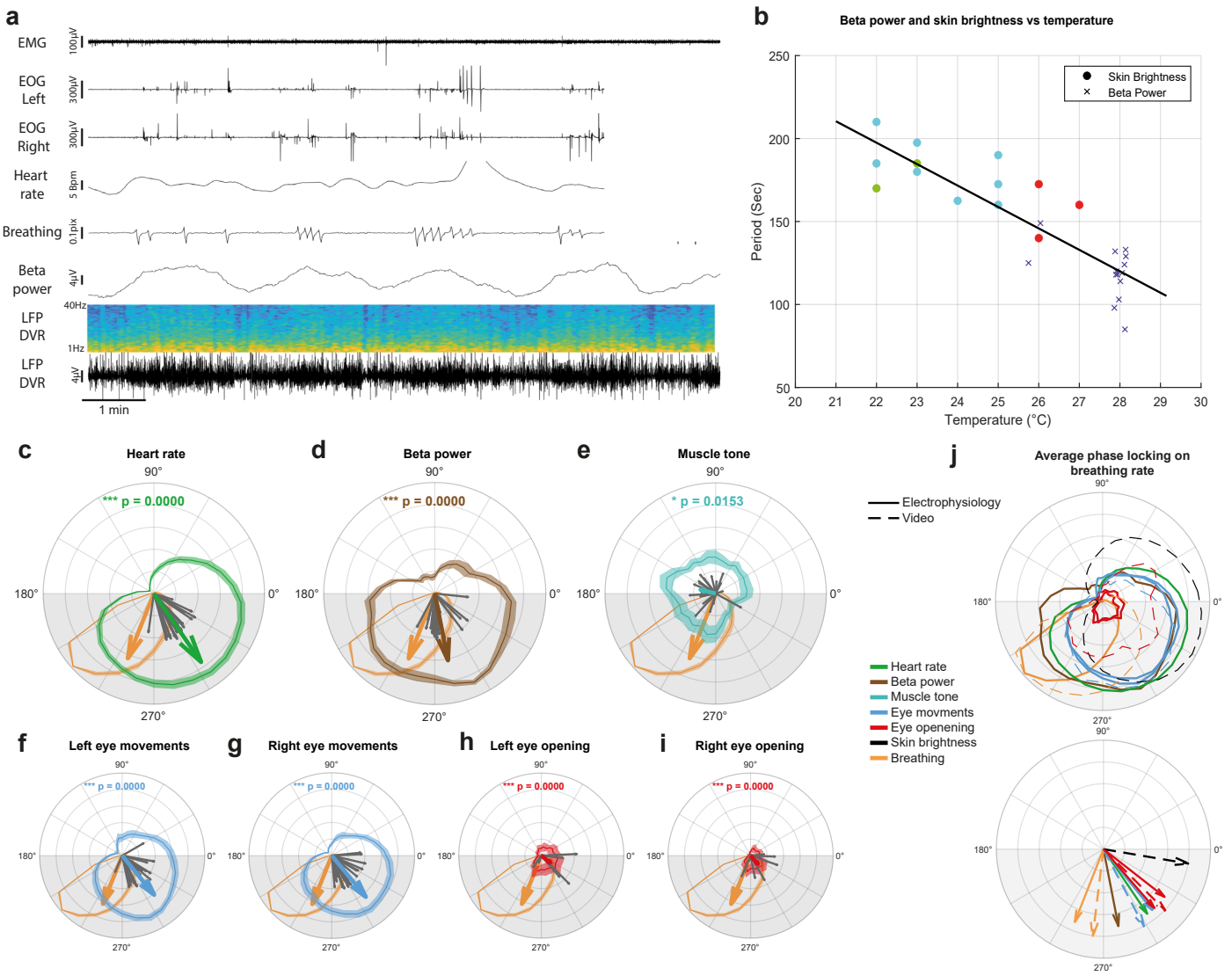

Extended Data Fig. 9 | Tight correlation between cerebral activity, physiology and skin brightness in sleeping chameleons. a, Ten-minute sleep recording. From the top to the bottom, electromyogram (EMG); left and right electrooculogram (EOG); heart rate; breathing movement; beta power (10–40 Hz); local field potential (LFP) recorded in the dorsal ventricular ridge (DVR) represented in the frequency (color-coded map, from low (blue) to high power (yellow)) and the corresponding raw LFP signal (lower trace). **b**, Correlation between the beta power and skin brightness period (from different individuals represented by color-coded dots) relative to the temperature, showing that the cerebral and skin brightness infraslow rhythms are both temperature-dependent. **c**–**i**, The heart rate (**c**), beta power (**d**), muscle tone (**e**), left (**f**) and right (**g**) eye movement density, left (**h**) and right (**i**) eye opening relative to the breathing rate phase of the chameleon that was recorded with electrophysiology. The orange curve shows breathing rate relative to its own phase. The colored curve and shading show the mean and s.e.m. over all sleep bouts for this chameleon. **j**, The skin brightness, eye movement density and eye-opening relative to the breathing rate phase on the three chameleons where skin brightness was evaluated. The blue curve shows the breathing rate variations relative to its own phase. The colored curve and shading show the mean and s.e.m. over all trials and chameleons. On subfigures **a**–**j**, the gray arrows show the mean vector for each sleep bout. The color-coded arrows represent the average of all mean vectors. The vector length has been doubled for clarification. The p values were computed using a Rayleigh test, evaluating the uniformity of the sleep bout phase distribution. **c**–**j**, The number of individuals and replicates (sleep bouts) per species is indicated in Supplementary Table 1 (row 'LFP/EEG', 'ECG', 'Breathing', 'EOG', 'EMG'). Phase-locking statistics were computed by testing the uniformity of the circular distribution using the Rayleigh test.

nature portfolio

Corresponding author(s): Libourel P.-A.

Last updated by author(s): 09/09/2025

Reporting Summary

Nature Portfolio wishes to improve the reproducibility of the work that we publish. This form provides structure for consistency and transparency in reporting. For further information on Nature Portfolio policies, see our Editorial Policies and the Editorial Policy Checklist.

Statistics

For all statistical analyses, confirm that the following items are present in the figure legend, table legend, main text, or Methods section.

n/a	Confirmed	
☐	☒	The exact sample size (*n*) for each experimental group/condition, given as a discrete number and unit of measurement
☐	☒	A statement on whether measurements were taken from distinct samples or whether the same sample was measured repeatedly
☐	☒	The statistical test(s) used AND whether they are one- or two-sided *Only common tests should be described solely by name; describe more complex techniques in the Methods section.*
☒	☐	A description of all covariates tested
☐	☒	A description of any assumptions or corrections, such as tests of normality and adjustment for multiple comparisons
☐	☒	A full description of the statistical parameters including central tendency (e.g. means) or other basic estimates (e.g. regression coefficient) AND variation (e.g. standard deviation) or associated estimates of uncertainty (e.g. confidence intervals)
☐	☒	For null hypothesis testing, the test statistic (e.g. *F*, *t*, *r*) with confidence intervals, effect sizes, degrees of freedom and *P* value noted *Give P values as exact values whenever suitable.*
☒	☐	For Bayesian analysis, information on the choice of priors and Markov chain Monte Carlo settings
☒	☐	For hierarchical and complex designs, identification of the appropriate level for tests and full reporting of outcomes
☒	☐	Estimates of effect sizes (e.g. Cohen's *d*, Pearson's *r*), indicating how they were calculated

Our web collection on statistics for biologists contains articles on many of the points above.

Software and code

Policy information about availability of computer code

Data collection	The data collection procedures and materials are discribed in the supplementary information
Data analysis	Matlab (Mathworks) version r2021a Python 3.9, OpenCV library

For manuscripts utilizing custom algorithms or software that are central to the research but not yet described in published literature, software must be made available to editors and reviewers. We strongly encourage code deposition in a community repository (e.g. GitHub). See the Nature Portfolio guidelines for submitting code & software for further information.

Data

Policy information about availability of data

All manuscripts must include a data availability statement. This statement should provide the following information, where applicable:

- Accession codes, unique identifiers, or web links for publicly available datasets
- A description of any restrictions on data availability
- For clinical datasets or third party data, please ensure that the statement adheres to our policy

Data will be available upon reasonable request.

Research involving human participants, their data, or biological material

Policy information about studies with human participants or human data. See also policy information about sex, gender (identity/presentation), and sexual orientation and race, ethnicity and racism.

Reporting on sex and gender	Gender was based on self-reporting and is shared with concent (i.e., demographical data are collected according to the study portocol). Since this comparative study focuses on the role of infraslow oscillations across several species from the evolutionary prospective, sex- and gender-based analyses in humans are out of the scope of the purpose of the study and therefore were not performed.
Reporting on race, ethnicity, or other socially relevant groupings	Since this comparative study is focuses on the role of infraslow oscillations across several species from the evolutionary prospective, socially relevant grouping in humans are out of the scope of the purpose of the study and therefore were not performed.
Population characteristics	The study included 18- to 85-year-old volunteers in a good or normal general health condition (Eastern Cooperative Oncology Group grade of 0-1). The following exclusion criteria were applied: known (i.e., self-reported or documented in medical records) pre-existing structural deformations of the brain (e.g., previous stroke), known progressive neurological diseases, known psychiatric diseases, concomitant benzodiazepine medication, drug or alcohol abuse, inability to follow study procedure, and pregnancy.
Recruitment	The participants were recruited from the community and from the patients of Sleep-Wake-Epilepsy center of the Inselspital, University Hospital of Bern.
Ethics oversight	Ethics committee of Canton of Bern (Switzerland)

Note that full information on the approval of the study protocol must also be provided in the manuscript.

Field-specific reporting

Please select the one below that is the best fit for your research. If you are not sure, read the appropriate sections before making your selection.

☒ Life sciences ☐ Behavioural & social sciences ☐ Ecological, evolutionary & environmental sciences

For a reference copy of the document with all sections, see nature.com/documents/nr-reporting-summary-flat.pdf

Life sciences study design

All studies must disclose on these points even when the disclosure is negative.

Sample size	No Statistical tests were used to predetermined sample sizes. We established that our sample sizes are sufficient based on previous experience and commonly used sample sizes in this field of research, taking into account the unusual nature and limited availibility of the animal species studied.
Data exclusions	Animals or trials with low signal to noise ratio, artefact or unstability in the LFP were excluded from the analysis.
Replication	We could replicate our results.
Randomization	Randomization were not relevant for our study.
Blinding	Our study was mostly decriptive without intervention on the normal behavior or physiology, blinding is not required. In addition, all the analysis were automatized, extraction of heart, eye and breathing peaks were checked visually for all trials.

Reporting for specific materials, systems and methods

We require information from authors about some types of materials, experimental systems and methods used in many studies. Here, indicate whether each material, system or method listed is relevant to your study. If you are not sure if a list item applies to your research, read the appropriate section before selecting a response.

Materials & experimental systems

n/a	Involved in the study
☒	☐ Antibodies
☒	☐ Eukaryotic cell lines
☒	☐ Palaeontology and archaeology
☐	☒ Animals and other organisms
☐	☒ Clinical data
☒	☐ Dual use research of concern
☒	☐ Plants

Methods

n/a	Involved in the study
☒	☐ ChIP-seq
☒	☐ Flow cytometry
☒	☐ MRI-based neuroimaging

Animals and other research organisms

Policy information about studies involving animals; ARRIVE guidelines recommended for reporting animal research, and Sex and Gender in Research

Laboratory animals	adult animals and humans (supplementary information)
Wild animals	All animals were obtained from official breeders and salers.
Reporting on sex	Animals have been chosen based on availibility, weight (age) and healthy appearance, irrespective of their sex. We did not perform any sex-based analysis, but our results are consistent across individuals and species.
Field-collected samples	This study did not involved wild animals.
Ethics oversight	All experimental procedures were approved by the relevant animal welfare authority. (Methods)

Note that full information on the approval of the study protocol must also be provided in the manuscript.

Clinical data

Policy information about clinical studies

All manuscripts should comply with the ICMJE guidelines for publication of clinical research and a completed CONSORT checklist must be included with all submissions.

Clinical trial registration	The observational study is registered at the ethics committee of Canton of Bern, Switzerland (KEK #2021-000726).
Study protocol	Available at: https://drive.google.com/file/d/1em_rLF48hkFMDmlbpueGHwovbumCxmDZ/view?usp=sharing
Data collection	Recruitment and data collection took place in 2021-2023 at the Sleep-Wake Epilepsy Center of the Inselspital, University Hospital of Bern. The written informed consent and the consent for the further use of the data was acquired from all study participants.
Outcomes	This manuscript presents tertiary outcomes of the observational study, focusing on the fundamental analysis of the associations between the parameters of sleep macro- and microarchitecture (i.e., infraslow oscillations).

Plants

Seed stocks	*Report on the source of all seed stocks or other plant material used. If applicable, state the seed stock centre and catalogue number. If plant specimens were collected from the field, describe the collection location, date and sampling procedures.*
Novel plant genotypes	*Describe the methods by which all novel plant genotypes were produced. This includes those generated by transgenic approaches, gene editing, chemical/radiation-based mutagenesis and hybridization. For transgenic lines, describe the transformation method, the number of independent lines analyzed and the generation upon which experiments were performed. For gene-edited lines, describe the editor used, the endogenous sequence targeted for editing, the targeting guide RNA sequence (if applicable) and how the editor was applied.*
Authentication	*Describe any authentication procedures for each seed stock used or novel genotype generated. Describe any experiments used to assess the effect of a mutation and, where applicable, how potential secondary effects (e.g. second site T-DNA insertions, mosiacism, off-target gene editing) were examined.*